12-1990

# Extension of the Metal Light Pipe Infrared Spectroscopy Technique: Applications to Surface Adsorption and High Tc Superconductors

Torsten Will
*Utah State University*

# EXTENSION OF THE METAL LIGHT PIPE INFRARED SPECTROSCOPY TECHNIQUE: APPLICATIONS TO SURFACE ADSORPTION AND HIGH $T_c$ SUPERCONDUCTORS

by

Torsten Will

A thesis submitted in partial fulfillment
of the requirements for the degree

of

MASTER OF SCIENCE

in

Physics

Approved:

| | |
|---|---|
| Major Professor | Committee Member |
| Committee Member | Dean of Graduate Studies |

Utah State University
Logan, Utah

1990

# ACKNOWLEDGMENT

It gives me great pleasure to acknowledge the help I have received during this research. I would like to thank Dr. John Robert Dennison for his advice and encouragement throughout the course of this research. His advice, guidance, and moral support were invaluable to the success of my work. I also wish to acknowledge Dr. Wilford N. Hansen for his valuable help and fruitful discussions and Dr. Jan Sojka who supported me selflessly during part of my work.

Among all the people who helped me during this work, I would especially like to thank Val King and Steve Dahsle from the Space Dynamics Laboratory for their knowledgeable advice and the countless occasions when we used their equipment. I would also like to thank Dr. John L. Hubbard for the use of his glove box and his help to start up our glove box.

To my friends (especially Teresa Ellen Elizabeth Burns, Michael Rosteck, and Liza Stacishin) I wish to say thanks for their moral support, encouragement, and the "good time" during my stay in Logan. Finally, I wish to express my gratitude to my friend, Elizabeta Stacishin de Moura, for her patience and support and the great time we had together.

Torsten Will

CONTENTS

# LIST OF TABLES

# LIST OF FIGURES

Figure Page

Figure Page

# ABSTRACT

Extension of the Metal Light Pipe Infrared Spectroscopy Technique: Applications to Surface Adsorption and High $T_c$ Superconductors

by

Torsten Will, Master of Science

Utah State University, 1990

Major Professor: Dr. John Robert Dennison
Department: Physics

The development of an infrared instrument for the study of surface adsorption and high $T_c$ superconductors is presented and its applicability is discussed. The use of and theoretical background for the metal light pipe multiple-reflection technique are discussed in comparison to other infrared devices. Measurements are carried out to determine its limitations with powdered substrates as well as its sensitivity limitation for thin films. The results of the two test measurements, adsorption of CO on MgO and investigation of the energy gap of high $T_c$ superconductors, are presented. Comparisons of the spectra with the experimental and theoretical literature are presented where possible. The necessity for simultaneous infrared and vapor pressure isotherm measurements is discussed, and

their instrumental realization is shown. Infrared measurements on the energy gap of high $T_c$ superconductors are shown and compared with results from the literature.

(117 pages)

# CHAPTER I

# INTRODUCTION

The purpose of this thesis research is to develop an infrared (ir) system that can measure spectra under controlled gas environments and cryogenic temperatures. The resulting data will lead to measurements of important quantities, such as the adsorbate-adsorbate interaction and the binding energy and binding structure of adsorbed gases on well-characterized crystal surfaces. These questions can be and have been addressed with methods other than ir [e.g., inelastic neutron scattering (INS) and electron energy loss spectroscopy (EELS)], but those methods require an extensive apparatus and do not have the high resolution and intensity that is provided by ir data. The ease of the measurements and the simplicity of the apparatus greatly favor the investigation of these problems with ir.

In our experimental set-up we used a metal light pipe (MLP) multiple-reflection technique to enhance the signal-to-noise ratio. The MLP technique was developed by Hansen *et al.*[14,15] and incorporates high throughput, multiple reflections, and a high signal-to-noise ratio. The extension of the technique to controlled gas and cryogenic temperature conditions is an essential improvement of the MLP for the study of a variety of interesting fields in physics. Chemisorption, as well as the proposed physisorption measurements, is tractable with the MLP; even

measurements of the energy gap of high $T_c$ superconductors ($HT_cS$) have been done with the MLP.

This thesis research, however, was limited to the design, construction, and initial test measurements of the new technique in order to establish it as a complementary surface analysis probe. We decided to test the instrumentation with two initial measurements, both of which have been done previously with ir devices other than the light pipe. Our intention was not simply to test the hardware and compare our results with those in the literature, but also to try to add to the existing data base. Infrared measurements of the energy gap of the high $T_c$ superconductor $YBa_2Cu_3O_7$ and the vibrational spectra of adsorbed carbon monoxide gas on magnesium oxide were chosen to fulfill this purpose. The data base for both experiments is broad enough for us to predict and compare our results, but there is still a lot of interesting physics yet to be discovered.

The measurements on $HT_cS$ should test the liquid helium and far-ir capabilities of the system, which are important for the measurements that are planned in the future. Infrared investigation of $HT_cSs$ is a standard technique in $HT_cS$ research, but the results are neither consistent nor conclusive. Because of our different approach, it might be possible to uncover some of the coupling or conduction mechanisms, which may help lead to an explanation of these

still mysterious materials. If, however, our technique is not able to show new features in the ir spectrum, at least it can add to the existing data about the energy gap of $HT_cS$, data that needs to be explained by any theory dealing with $HT_cS$. Regardless of the disagreement in the existing measurements, we were able to use $HT_cS$ as a test because all the measurements showed an increase in reflectivity when a material turns superconducting, disagreeing only on the size of the energy gap. Since $HT_cS$ are usually produced as powders, it was our hope to get better measurements because the light pipe can use those powders directly instead of using a sintered disc.

The adsorption of CO on MgO, however, is an interesting problem in surface science for several reasons. It can be approached from two major research fields. From the chemical viewpoint, CO adsorbed on MgO is already intensively studied because MgO has a very large surface area and is therefore used as a catalyst. From the viewpoint of surface physics, however, MgO represents a new class of high-surface-area crystals for study of the binding energy between gases and crystals. Because of its square-substrate-crystal structure, it should lead to an understanding of the binding potential of polar or nonpolar molecules on square lattices instead of the more common hexagonal lattices found, for example, in graphite or laminar halides.

The initial measurements of CO on MgO, however, should primarily test how the MLP reacts to a gas environment under liquid nitrogen conditions in the mid-ir region, and should determine if the light pipe is sensitive to gases adsorbed on powders. Experimental and theoretical investigation of adsorbed CO on MgO showed consistency, but did not investigate problems such as CO-CO interaction and CO adsorbed on defects. We will, therefore, begin our measurements of gases adsorbed on a substrate with the adsorption of CO on MgO to verify that this new technique is indeed a complementary technique to INS and EELS to study the dynamics of adsorbed species.

Despite the variety of uses of the MLP, we plan to focus mainly on the investigation of adsorbed gases on crystalline powders. Our long-term expectations for this instrument will be the investigation of problems such as phase transitions, two-dimensional melting, and low-energy-collective phonon excitations of gases adsorbed on powders. These measurements require liquid helium capability under controlled gas environments and require far- and mid-ir measurements. The research presented here should be seen as the second step leading to those measurements, following the initial development of the MLP.

This thesis is structured in the following way. First, I will give a description of the instrumentation designed for these experiments. A literature review that

should enable the reader to evaluate our measurements will follow. The review also provides necessary background and places the presented research in the context of the surrounding fields of surface science. Chap. IV will present and discuss the data and compare it with results from the literature. Chap. V will then conclude and summarize the main facts of the thesis and recommend further use and fields of investigation for our technique.

# CHAPTER II

## EXPERIMENTAL DESIGN

The system that I am going to describe was designed to measure infrared spectra under controlled gas and cryogenic temperature conditions. It uses a metal light pipe technique similar to fiber optics and should lead to the binding energy of gases adsorbed on high-surface-area substrates, as well as to the energy gap of high $T_c$ superconductors. The design should incorporate high signal-to-noise ratio, and should give rise to a strong ir signal from the adsorbate or high $T_c$ superconductor in question.

To best serve our short-term and long-term needs, the experimental design was divided into four interrelated parts. Each component serves a different purpose in this experiment and is independently applicable for other experiments. For the short-term requirements of the adsorption of CO on MgO and the high $T_c$ superconductor measurements, the components are connected and used in the following way.

The gas handling system (Chap. II, Sec. B) provides the controlled gas environment for the adsorption of gaseous adsorbates on solid substrate and measures the coverage of the adsorbate on the substrate in the light pipe. The measurement of the energy gap of high $T_c$

superconductors does not use this component, since no gas is adsorbed. The dewar and the temperature-control unit (Chap. II, Sec. B) supply a controlled temperature environment for the light pipe. The light pipe (Chap. II, Sec. C) is used for simultaneous coverage and ir measurements of the adsorption of CO on MgO and as an ir cell for the $HT_cS$ energy gap measurements. The Bruker spectrometer, with the associated optics (Chap. II, Sec. D), is the instrument used to record the ir spectra.

Each of the following sections includes a description of parts, the use of the apparatus, and the physical principles underlying each component. The sources, design details, and calibration procedures are presented in the appendices, as are longer calculations.

## A. Gas Handling System

The gas handling system is used to determine the surface area of the substrate and the coverage of the gas on the substrate. It uses a technique called vapor pressure isotherm (VPI) to determine both quantities. A VPI relates the amount of gas adsorbed on the substrate to the equilibrium pressure of the residual gas in the gas phase. The coverage of a certain gas on a given substrate is well defined at a given temperature and equilibrium pressure. In a later section of this chapter, I will

explain thoroughly how a VPI is measured and how it will lead to the coverage of the gas on the substrate.

It is possible to get far more thermodynamic information from a VPI than just the surface area of the substrate and the coverage of the adsorbate. The data can yield information[28,31] such as the isosteric heat of adsorption $q$ and the isothermal compressibility $K_T$.

A gas handling system does not have the capability of directly measuring the number of molecules adsorbed on the adsorbent. The only measurable physical quantity is the equilibrium pressure of the residual gas in the sample cell and manifold. The number of gas particles at the equilibrium pressure can then be determined from the ideal gas law if the temperature and volume are known. At the beginning, the gas is put just in the manifold, and the pressure is recorded. After that, the gas is released in the sample cell, and the pressure is again recorded after the system has equilibrated. The difference of molecules in the gas phase before and after the adsorption is then calculated in the following way:

$$n_i = (P_f\ V_g)\ /\ (R\ T_g), \tag{1}$$

$$n_f = P_f/R\ (V_g/T_g + V_d/T_g + V'_d/T_s), \tag{2}$$

and

$$n_{ads} = n_i - n_f, \tag{3}$$

where $n_i$ is the initial number, $n_f$ is the final number of molecules in the gas phases, and $n_{ads}$ the adsorbed number of molecules on the surface. The initial pressure in the gas handling system is given by $P_i$ and the final pressure by $P_f$, while $R$ is the ideal gas constant. $T_g$ is temperature of the gas handling system, and $T_s$ is the temperature of the sample. $V'_d$ represents the dead volume at the sample temperature, $V_d$ is the dead volume at the gas handling system temperature, and $V_g$ is volume of the gas handling system.

Therefore, $n_{ads}$ determines how many molecules have been adsorbed. For the final number of molecules in the gas phase there is a correction to the volume because the volume of the sample cell is added to the volume of the gas handling system, which gives a drop in the pressure even without any adsorption of the gas. This so called "dead volume" is usually calibrated at room and cryogenic sample temperatures with helium. Helium is the standard gas for any calibration since it does not adsorb appreciably at temperatures above 5 K. The calibration at both temperatures is necessary because the dead volume is not at a uniform temperature. Eq.(2) corrects this problem by assuming two volumes, one at the gas handling temperature and the other one at the sample temperature. If, however, the sample temperature is different from the temperature that the dead volume was calibrated with, there will be an

error in $n_{ads}$. This error will, however, be much smaller than with only one temperature measurement for the dead volume.

As shown later in this section, the primary force for the physisorption of gases on surfaces is a weak van der Waals interaction between the surface and the gas molecule. The resulting binding energy is usually of the order of several meV. The molecular internal energy $U$, however, acts to desorb the molecule from the surface and is a function of the temperature. The general dependence of the amount adsorbed is

$$n_{ads} \quad exp\ (U(T) - E_b)\ /\ k_B T, \tag{4}$$

where $n_{ads}$ is the number of adsorbed molecules, $U(T)$ is the internal energy, $E_b$ is the binding energy, $k_B$ is the Boltzmann constant, and $T$ is the temperature. The temperature at which the gas can be adsorbed on the surface depends, therefore, on the substrate, the gas, and the temperature. Since the substrate and gas are usually not changed during a VPI, one only has to watch the temperature. It is not only important for the sample temperature to be low, but it is also important for the temperature to be held constant during the VPI since the equilibrium pressure for a completed layer depends approximately exponentially on the temperature [Eq. (4)].

The theoretical background for the adsorption of gases on well-defined crystals has been established and tested. Gevirzman *et al.*[10] derived an equation based on classical electrostatics to describe the binding potential of an ionic crystal with an adsorbate. Their equation consists of five potential terms up to the order of a quadrupole interaction for a single adsorbed molecule with the surface. The total potential is given as[10]

$$\phi_{TOTAL} = \phi_{VDW} + \phi_{REP} + \phi_{IND} + \phi_{PD} + \phi_{Q}, \qquad (5)$$

where $\phi_{VDW}$ is a dipole-dipole force between the adsorbed molecule and the surface, which varies with distance $r$ as $1/r^6$; $\phi_{REP}$ is a repulsive force due to an overlap of electron clouds of the surface ions and the adsorbate, which varies with distances as $exp\ (-ar)$; $\phi_{IND}$ is a potential due to the induced dipole in the adsorbed molecule, which depends on the adsorbates polarizability; $\phi_{PD}$ is a potential, which depends on the permanent electrostatic dipole of the adsorbate; and $\phi_{Q}$ is a potential due to the quadrupole moment of the molecule

A general result of Eq. (5) is that molecules close to the surface experience a larger magnitude of the surface potential than molecules farther away from the surface. Fig. 1(a) shows a simplified diagram of the surface potential versus the distance from the substrate, and Fig. 1(b) shows a simplified VPI. The total energy that is

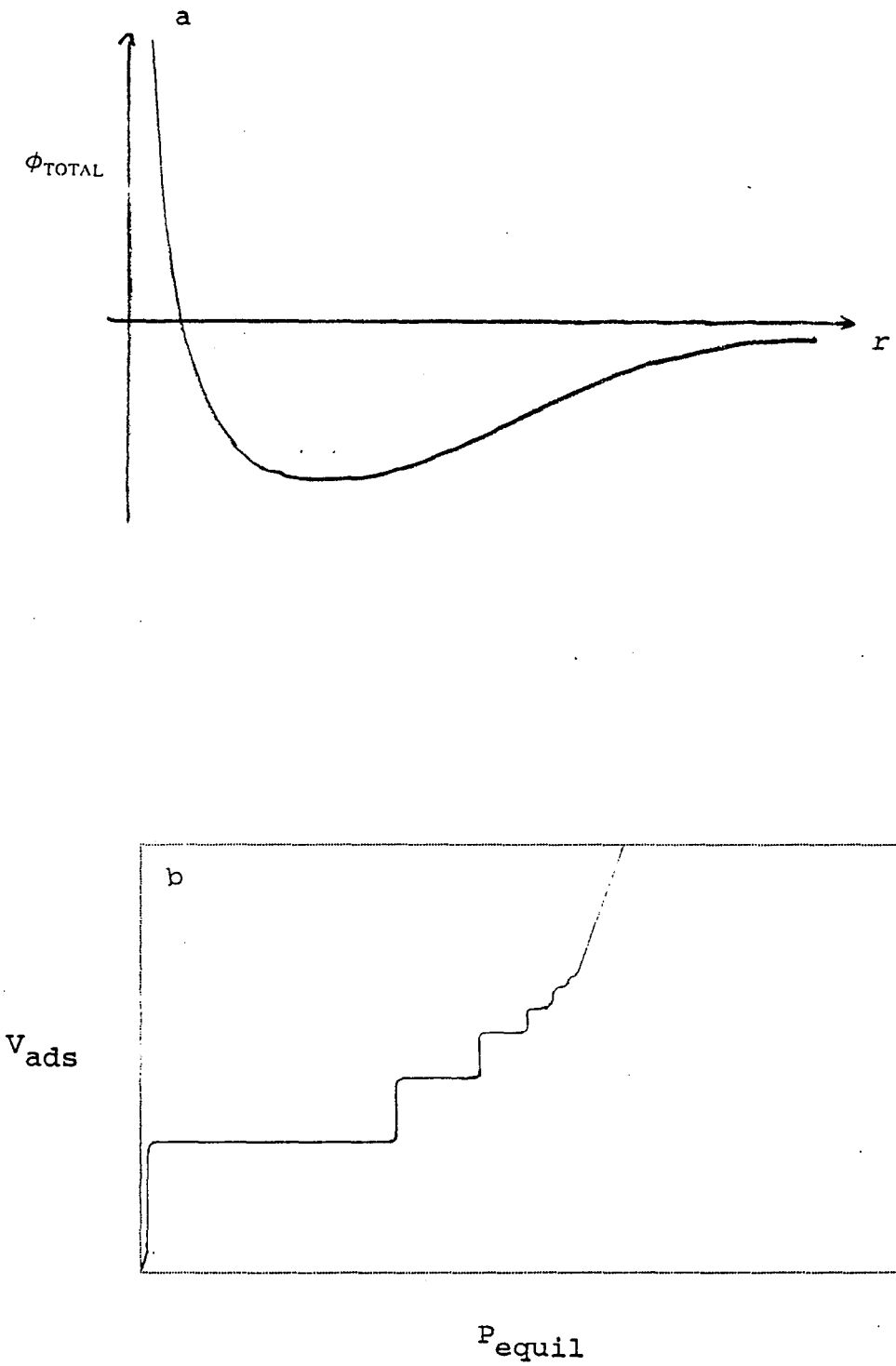


FIG. 1. (a) Graph of the surface potential experienced by an isolated gas molecule and (b) corresponding ideal VPI.

required to adsorb a molecule on the surface is the same for any layer. The surface potential and the chemical potential are the two energies that add up to the total energy. One can see that the first layer experiences a larger magnitude of the surface potential and needs, therefore, less chemical potential from the gas to adsorb on the surface. Since the second layer is farther away from the surface, it has a smaller magnitude of the surface potential and requires, therefore, a larger chemical potential, which corresponds to a higher pressure. In a $n_{ads}$ versus $P_f$ diagram, the first layer is, therefore, formed at lower pressures than the second. This fact is used to determine the coverage of a substrate on the surface because a VPI will not be a smooth function, but rather will show steps in a $n_{ads}$ versus $P_f$ diagram. The first layer will experience the highest magnitude of the surface potential, and, therefore, will be filled at the lowest pressure. In that environment, most particles are added to the surface (since the surface potential is almost the same) and very few are added to the gas phase. This corresponds in the $n_{ads}$ - $P_f$ diagram to a very high slope of the graph. The molecules that are added to the gas phase compensate for a small additional energy that is originated because the gas molecules repel each other as the coverage increases. Another reason is that for a nonperfect substrate, defects in the substrate will be occupied at a

slightly different pressure due to the different surface potential.

For an ideal gas and a perfect substrate it would be different, and one could add particles at a well-defined pressure, without raising the pressure, until a layer is completed. After the completion of the first layer, most of the particles are then added to the gas phase while few are added to the surface. The increase in pressure provides the gas molecules with a larger chemical potential because the magnitude of the surface potential is smaller due to a lager distance from the surface. This corresponds in the $n_{ads}$ - $P_f$ diagram to regions with a low slope. When the increase in pressure is high enough, the gas will start to form the second layer, which will show again a high slope in the $n_{ads}$ - $P_f$ diagram. The pressure increase during a new layer formation is much smaller than the pressure increase between a layer formation. For an ideal gas and a perfect sample, it would again be a little different because no molecule would be added to the surface until the pressure was high enough to start the second layer at a well-defined pressure. Fig. 2(a) shows a VPI of nitrogen on graphite and Fig. 2(b) one of CO on MgO. The regions with low and high slope are well defined so that an analysis is fairly easy. There are several methods for determining when formation of a layer is finished, and all of them give a slightly different result.

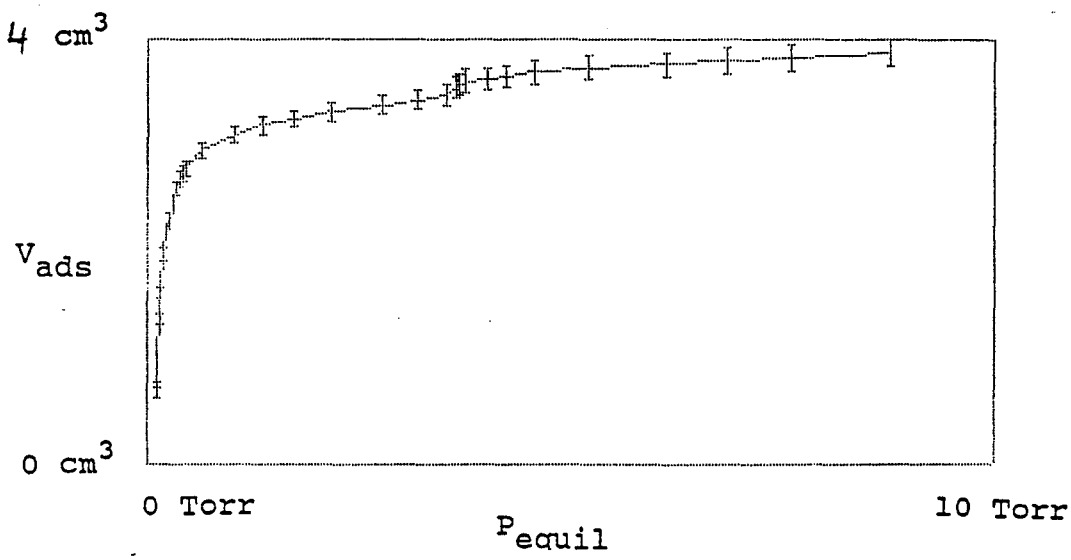


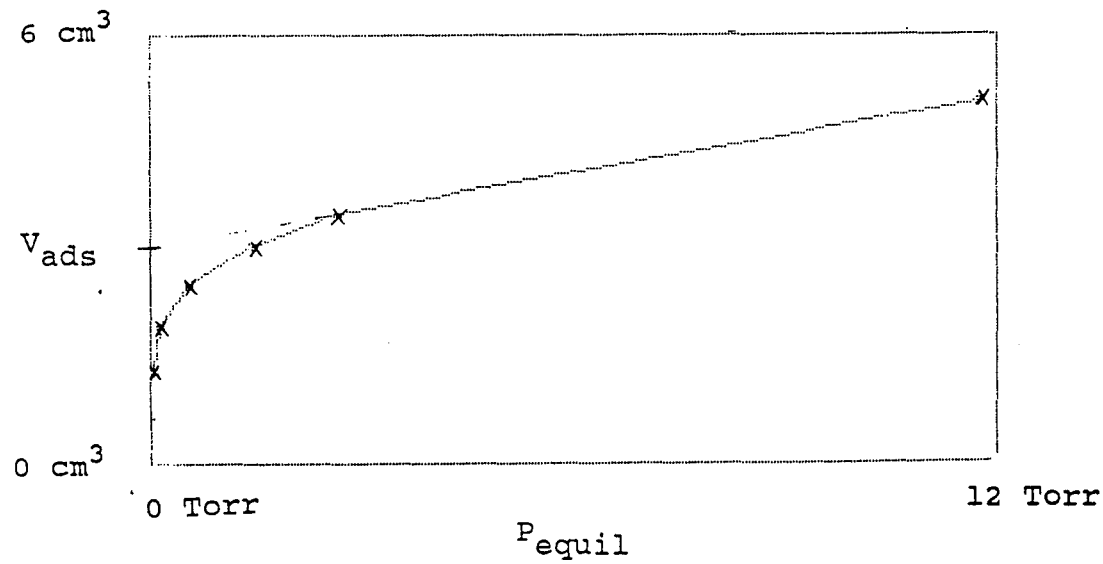


FIG. 2. VPI of (a) $N_2$ on 0.67 g of graphite at 78 K and (b) CO on 0.5 g of Puratonic MgO at 89 K

Young and Corwell[33] provide a thorough discussion of the methods. Furuyama *et al.*[8] compare the two major methods, the BET and the B-point methods, in the context of adsorption of CO on MgO. The differences originate in the nonideal gas properties, which do not show infinite and zero slopes. It is possible that a real gas forms the second and third layer before it completes the first layer, or that it forms bulk after it has formed only one or two layers.

The B-point method determines the point in the $n_{ads}$ - $P_f$ diagram where the graph starts to become linear [Fig. 2(b)]. This point is identified as the point where the adsorption changes from predominant adsorption in the first layer to predominant adsorption in the second layer. From this point, a line with the same slope is drawn which intercepts the line of zero pressure at $V_{ads}$. A $V_{ads}$ - $P_f$ diagram is a different way to display the data of a VPI. $V_m$ is called the volume of gas required to fill a monolayer in standard $cm^3$. Any submonolayer coverage is evaluated as the ratio of the adsorbed volume divided by $V_m$. This method requires many points in a VPI to determine the B-point exactly.[33] The BET method, however, tries to avoid the problem of many data points by analytically locating the B-point. One modification of the BET method requires only one data point to locate monolayer volume. The tradeoff for this advantage is lost accuracy, if the graph does not

bend sharply or is at high relative pressures (relative pressure is defined as the equilibrium pressure divided by the saturation vapor pressure at that temperature). It is also possible to calculate monolayer volumes with the BET method even though the data do not show a well-defined plateau at all and the B-point method would not allow the determination of a monolayer volume.[33] The BET method can also lead to negative interception with the abscissa if relative pressures higher than 0.2 are used. This would imply a negative monolayer volume. All these disadvantages are usually avoided if one uses substrates with a high surface area[33] that have a monolayer completion at relative pressure less than 0.2. In fact, Furuyama *et al.*[8] determined the surface area for MgO within 10% of each other using both methods by using small relative pressures.

The preferred procedure used to record a VPI is the following: Initially the gas handling system and light pipe are carefully pumped out for more than 12 hours to a pressure of less than $10^{-3}$ Torr. To achieve a cleaner substrate, the sample is also heated up to 70° C during the pump out to drive off residual water from the cell. It is then necessary to calibrate the dead volume of the sample cell at room and sample temperatures. The actual vapor pressure isotherm is begun by introducing the adsorbate in the gas handling system and recording the pressure $P_f$ (typically several Torr). The gas is than released into

the sample cell, and after the system is equilibrated (usually after 1 to 2 hours), the final equilibrium pressure is again recorded. Additional gas is added by repeating the last two steps until the isotherm is completed. A computer program was developed to record and display the vapor pressure isotherm and to perform the necessary calculations.

In summary, we drew the following conclusions for the present design of the gas handling system and the use of the sample. The calibration of any volumes needs to be done as carefully as possible. The temperature of the sample cell and the gas handling system needs to be as stable as possible, while the use of a highly accurate capacitance manometer is essential for a good isotherm. At present, the volumes of the gas handling system are calibrated within an error of less than 0.3%. It is possible to keep the sample cell within +0.5 K and -1.5 K of the desired temperature, while the change in the temperature of the gas handling system is determined by the changes in the room temperature. The capacitance manometer is accurate to +/- 0.01 Torr. In Appendix A the calibration procedure and the error analysis are explained in greater detail.

B. Dewar and Temperature Controller

The dewar with the connected temperature controller comprise the unit that keeps the sample cell at a desired temperature--in a range between 30 K and 350 K. The dewar (Fig. 3) is filled with suitable cryogens, such as liquid helium or nitrogen, to provide approximately the desired temperature. The sample cell is connected to the cold surface with a 5 cm aluminum extension, which provides good thermal contact. Layers of insulation can be added between the cold surface and the extension to build up a temperature gradient between the light pipe and the liquid cryogens.

Attached heaters heat the sample to intermediate temperatures. Fig. 4 shows a block diagram of the apparatus used to control the temperature. The power to the 50 Ohm resistive heaters is controlled by a standard temperature controller (Omega model CN 9121) that can operate in three different modes. At present, the controller operates in its simplest mode, an on/off signal. This mode provides a temperature stability of +0.5 K and -1.5 K. The controller can later run in either derivative or integral mode, which should provide a temperature stability of +/- 0.1 K.

The dewar was purchased from Kadel Engineering and has been slightly modified at the extension. It has been leak tested to a leak rate below $1.5 \times 10^{-9}$ standard $cm^3$ helium

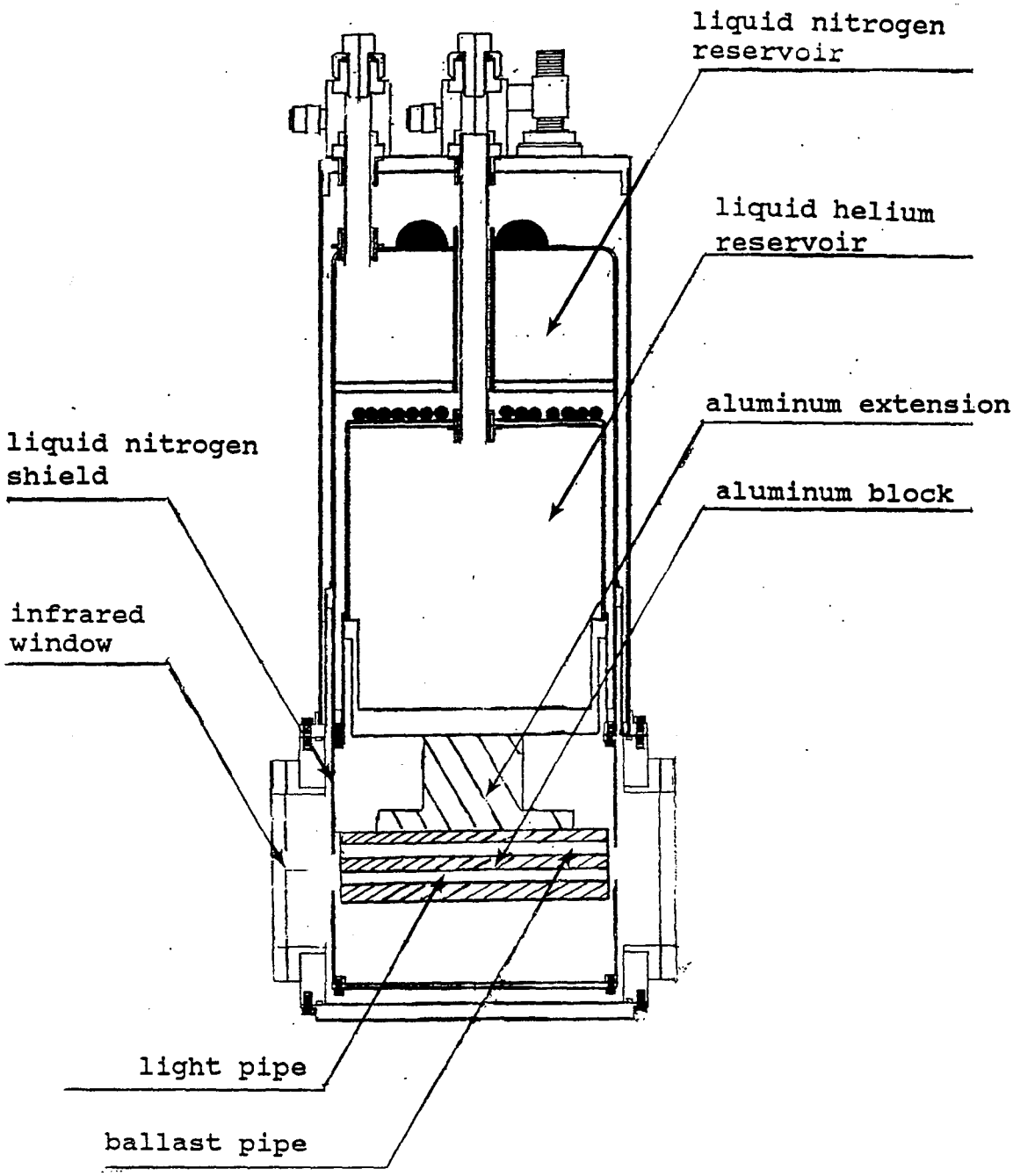


FIG. 3. Schematic of the liquid helium cryostat with the light pipe.

per sec and reaches pressures below $10^{-3}$ Torr at room temperature. The dewar offers two large windows for the incoming ir beam, and four ports for additional feedthroughs, for example, the gas inlet tube or the electrical feedthrough for heaters. Fig. 3 shows the dewar with the infrared windows and the attached light pipe. The dewar is designed for liquid helium applications; liquid nitrogen is used to cool the radiation shield. The minimum temperature attained to date for this design is 30 K. This is limited by the size of the light pipe and heat leaks. The heat leaks also determine the holding time for the shield and the cold surface itself. There are four major sources that determine the heat leaks: (1) thermal conduction due to residual gas in the dewar, (2) the radiative heat losses, (3) conduction through electrical and gas feedthroughs, and (4) the power deposited in the light pipe by the incoming ir beam. Appendix B contains detailed calculations of these heat losses. Based on those calculations, the radiation shield should have a holding time of 15 hours, which agrees very well with the experimental holding time. When the sample is at liquid nitrogen temperature, the theoretical holding time is 6 days. This has not been measured, but, experimentally, it exceeds 2 days. If the sample, however, is at liquid helium temperature and the radiation shield is filled with liquid nitrogen, the calculated holding time is 4 hours.

This is in reasonable agreement with preliminary measurements that indicate a holding time of 3.5 hours.

The temperature controller (Fig. 4) is capable of reading several sensors, such as a platinum resistance thermometer (RTD) and thermocouples. Since the controller is limited to 173 K, using a platinum resistance thermometer, a 100 Ohm resistor is placed in series at low temperatures. Above 78 K it is possible to simply use a standard resistance versus temperature table,[22] while one needs to calibrate the RTD below liquid nitrogen temperature. The other type of sensor used for the low temperature measurement was a type-T thermocouple. Above 80 K a type-T thermocouple shows a good response of the thermovoltage per degree; its response decreases at lower temperature. Its thermopower can be related directly to a temperature by using standard tables[22]. At the moment the sensors are precise within +/- 1 K, but the precision could be improved to +/- 0.2 K if the sensors are calibrated with a standard sensor.

## C. The Light Pipe

The light pipe (Fig. 5) is used as a sample cell for the ir measurements and the adsorption measurements at the same time. Based on the previous work by Hansen,[13,14,15] the adopted aspects in the design were the following: The light pipe had to be made with a highly ir reflecting

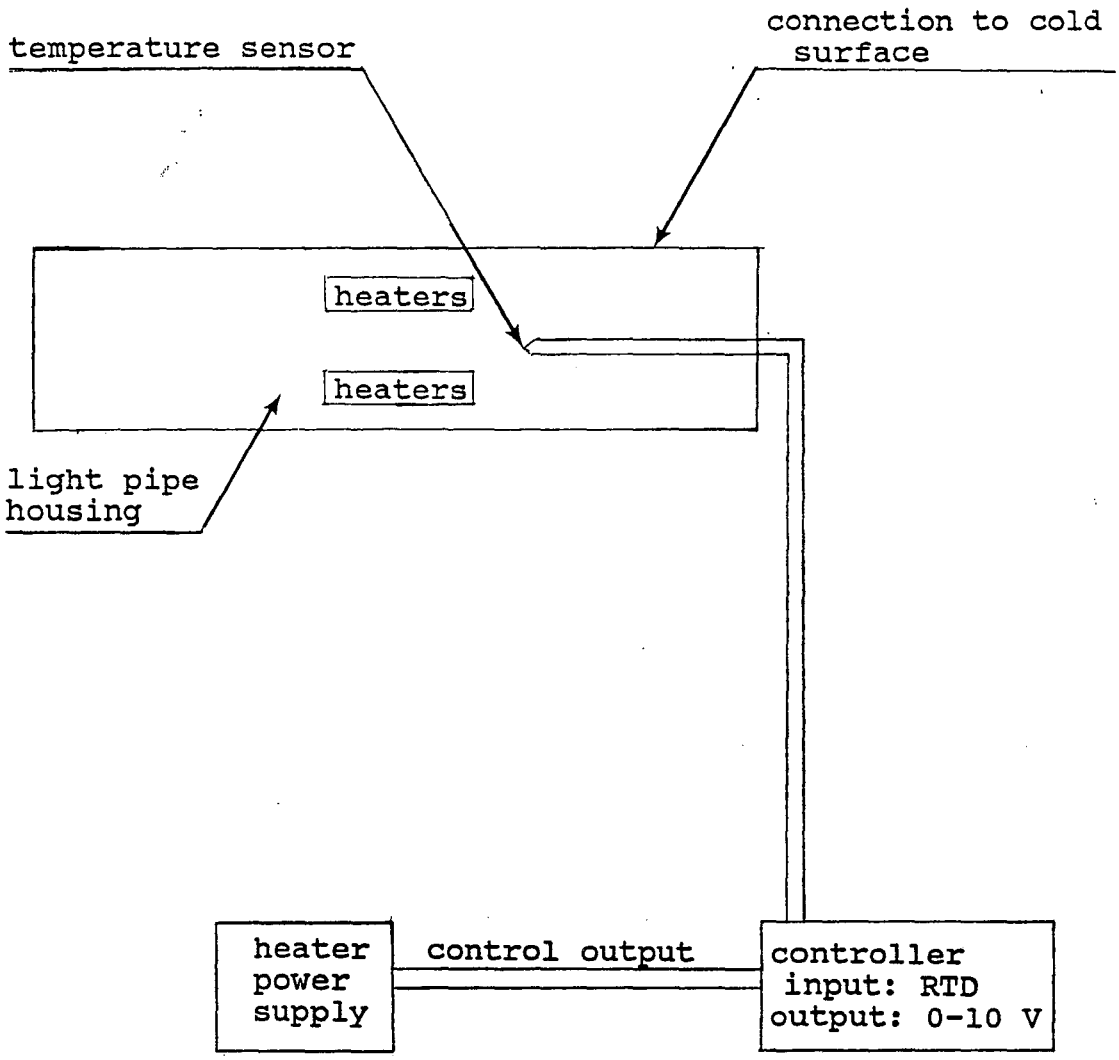


FIG. 4. Block diagram of the temperature controller unit.

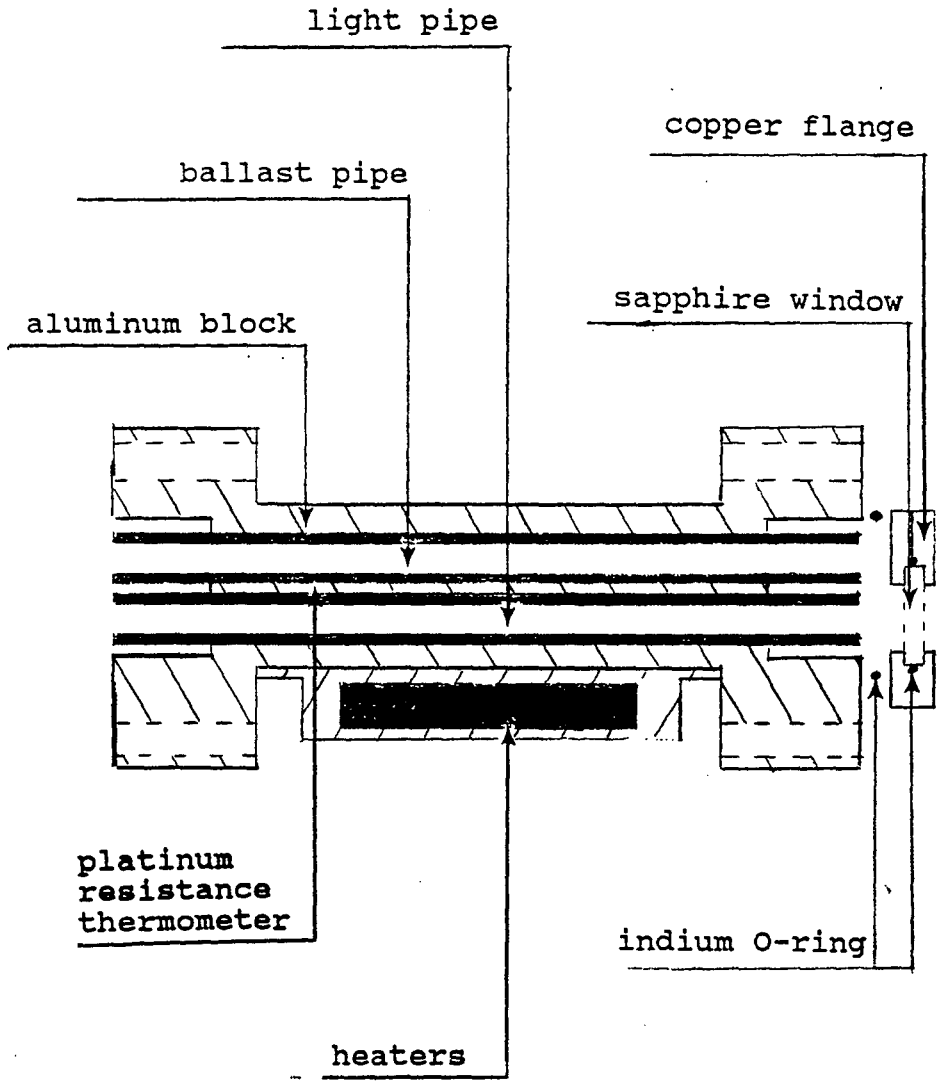


FIG. 5. Schematic of the metal light pipe with the aluminum block, ir windows, and heating unit.

material, such as polished copper, and should have been gold plated. Early tries did not show much difference in the throughput between a copper and a gold-plated copper pipe, but gold plating should prevent the copper from oxidizing. Polishing and gold plating produced a throughput of about 75%, ratioed to the throughput of no device in the spectrometer. Also, following the previous work, it was necessary to reach a high number of reflections while using a large angle of incidence (the angle between the light pipe surface normal and the incoming beam). The number of reflections increases the signal-to-noise ratio, while (as shown later) a grazing angle would enhance the effective electric field and therefore also boost the signal.

The light pipe is, however, restricted to the size of the cryostat, which limited the light pipe's length to 12 cm. Another important criteria in the design was the ease of assembly of the light pipe, because the sample handling and preparation for the adsorption work requires several precautions, and the assembly of the cell requires a glove box.

All the parts that are connected to the vacuum environment are usually baked in a vacuum furnace at 500° C at pressures less than $10^{-3}$ Torr. The sample is baked in the same furnace between 800° and 1000° C. All these components are then transferred into a nitrogen glove box,

where they are assembled. The bakeout at 500° C serves simply to clean the sample cell and to drive water off from the cell. The bakeout at 1000° C, however, should clean and anneal the substrate. It has been shown[5] that a bakeout at 1000° C does reduce the surface defects of MgO and enlarges its coherence length. Since the handling and assembly of any sample cell should be done with greatest care, it will be even more difficult to assemble the light pipe vacuum tightly in a glove box. Therefore, it should be as simple to assemble as possible. The glove box is usually clean to several parts per million of oxygen and water so that no additional contaminations and water are introduced after the bakeout. Water would destroy the surface of MgO, which is highly hygroscopic.[26]

Since the adsorption work also requires a controlled gas environment, even at low temperatures, sapphire windows with indium O-rings were used.[20] The cryogenic sapphire windows limit the light pipe at the present time to a wavenumber above 1650 $cm^{-1}$, which is good enough for the measurements of CO on MgO. Early tries with KBr or NaCl did not stand the pressure from the indium seals and could not stand the thermal shock of the cryogens. For the far-ir measurements on high $T_c$ superconductors, however, we use polyethylene windows with a knife edge as a seal.

One of our major goals was to measure the VPIs simultaneously with the ir spectrum. A ballast pipe with

several 100 mg of substrate was therefore placed close to the light pipe to ensure the same experimental conditions for substrate in the ballast pipe and the light pipe. One could determine the coverage from the equilibrium pressure data from a calibration curve taken earlier; this method does not use a ballast pipe at all and is used by several scientists.[24,34] However, we decided against this method because experimental conditions are crucial. As mentioned earlier, the equilibrium pressure scales exponentially with the temperature of the cell. The ballast pipe in Fig. 5 serves for the adsorption measurements only and is, as the light pipe, 10 cm long with an ID of 3 mm. The ballast pipe is completely filled with adsorbate to provide as much surface area as possible. The light pipe, however, is just dusted with the adsorbate so that the infrared beam can penetrate through it and reflect several times off the inside walls before it leaves the light pipe.

The effect of the substrate on the spectrum of the light pipe is presented in Chap. II, Sec. B, where the actual data are discussed. The effect of the substrate is one of the biggest problems in the whole set-up and is not completely solved. One would like to get as much adsorbate as possible in the light pipe to enhance the signal, but the throughput drops, in some case drastically, resulting in layers as small as 0.2 microns in effective thickness. There has to be a trade off between the throughput and the

signal of the adsorbed gas. The signal scales exponentially with the amount of adsorbent in the light pipe, while the throughput of the light pipe scales inverse exponentially with the amount of adsorbent in the light pipe. Several substrates, such as graphite, adsorb the ir beam almost perfectly, even at very low coverage, and let only the straight-through rays (rays that do not reflect off a wall at all) through. This changes the ratio of the gas phase molecules versus the adsorbed molecules in favor of the gas phase molecules, which makes, at present, an investigation of a graphite system almost impossible. Even adsorbents that have the same chemical stoichiometry act differently depending on their preparation, size, and impurities. The particles in the light pipe need, therefore, to be as small, as uniform, and as pure as possible to avoid scattering.[13,14,15] However, one is limited to insulators to avoid reflection and to penetrate through the particles. If the ir beam cannot penetrate through the adsorbent, the whole idea of a high-surface area substrate is invalid for the enhancement of the ir spectrum since the adsorbed particles on the shadowed side of the substrate cannot be excited by the ir beam. In Chap. 4 the transmittance of the ir beam is given for several samples, and there is also a discussion of the effect of such powders in the light pipe.

Fig. 6 shows how an outside ray of the light cone travels through the light pipe. One can see that the light pipe transfers the focal point and that there will be some skew rays. Skew rays will bounce in the light pipe and follow a screw path. The angles are higher than for meridional rays and theoretically much more difficult to treat.

To enhance the reflectivity and to increase the electric field just outside the surface, one can gold plate the inside of the light pipe. At the present stage of this research, this would not be economical, and gold and copper act very similarly. Fig. 7 shows the numerical result of the ratio of the parallel electric field just outside the surface versus the parallel electric field farther away from the surface for copper and gold as a function of the incident angle for a given wavelength. One can see that the most favorable region of the incident angle (angle between the surface normal and the beam) is between 60 degrees and 87 degrees. Since the light pipe is 10 cm long and 3 mm in diameter, it will reach up to 7 reflections for an incident angle between 82 degrees and 90 degrees. This locates the optics around the maximum of Fig. 7, which enhances the signal of the spectrum. This treatment does not take skew rays into account with their larger angle of incidence and more reflections. There exists no formula that treats these rays, since they might exceed the maximum

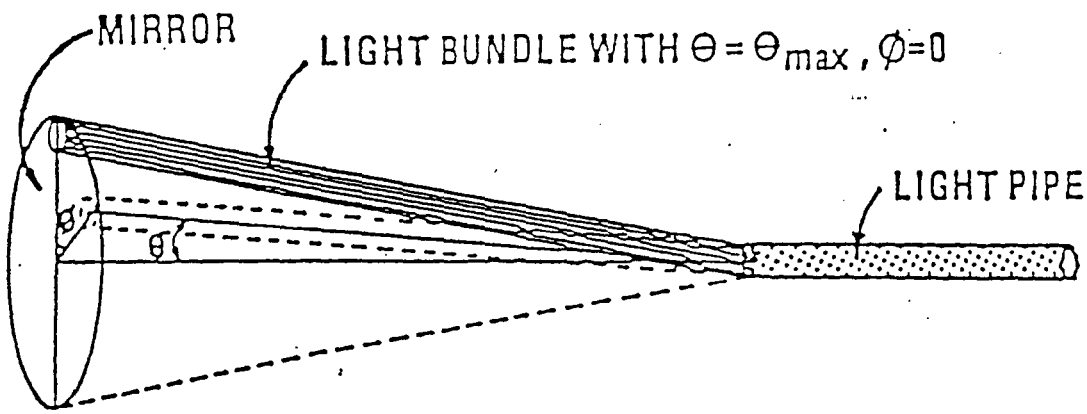


FIG. 6. Path of a bundle of incoming rays through the light pipe.[14]

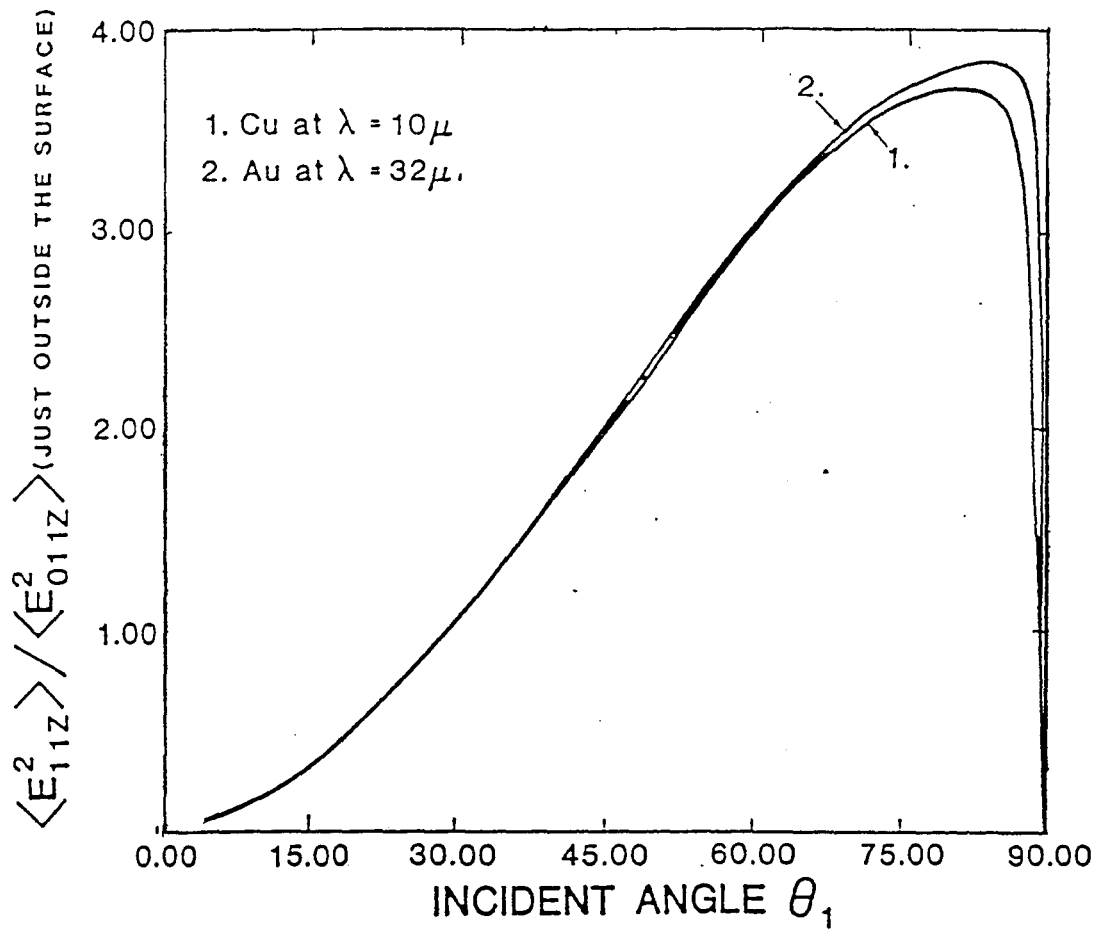


FIG. 7. Mean square electric field just outside a copper or gold surface, normalized to the incoming beam.[14]

and fall in the undesirable region above 88 degrees. However, a clean light pipe showed a good throughput in the mid-ir region (75%), while it acted poorly in the far ir region (10%). This was not expected and is inconsistent with the physical understanding; absorption due to scattering and due to the metal of the light pipe should be much smaller in the far-ir than the mid-ir region.[13,14,15] One possible explanation is that it is much more difficult to align the system in the far-ir region, and it was not possible to determine the correct adjustment parameters. Fig. 8(a) shows a 5 A film of silicone oil in the light pipe. Fig. 9 shows the same size film on a Grazing Angle Multiple Reflection (GMR) device. The GMR reaches 16 reflections and is specially designed for this type of data. One can see that the GMR exceeds the sensitivity of the light pipe in its designed application, but the light pipe still reaches a satisfying result. Fig. 10(a) displays the spectrum of a 30 A film of silicone oil, while Fig. 10(b) shows the spectrum from a single reflection device. The comparison demonstrates very well the effect of the light pipe.

### D. The Optical Path and the Spectrometer

The Fourier Transform Infrared (FTIR) spectrometer that is used for the data acquisition is a Bruker 113 V.

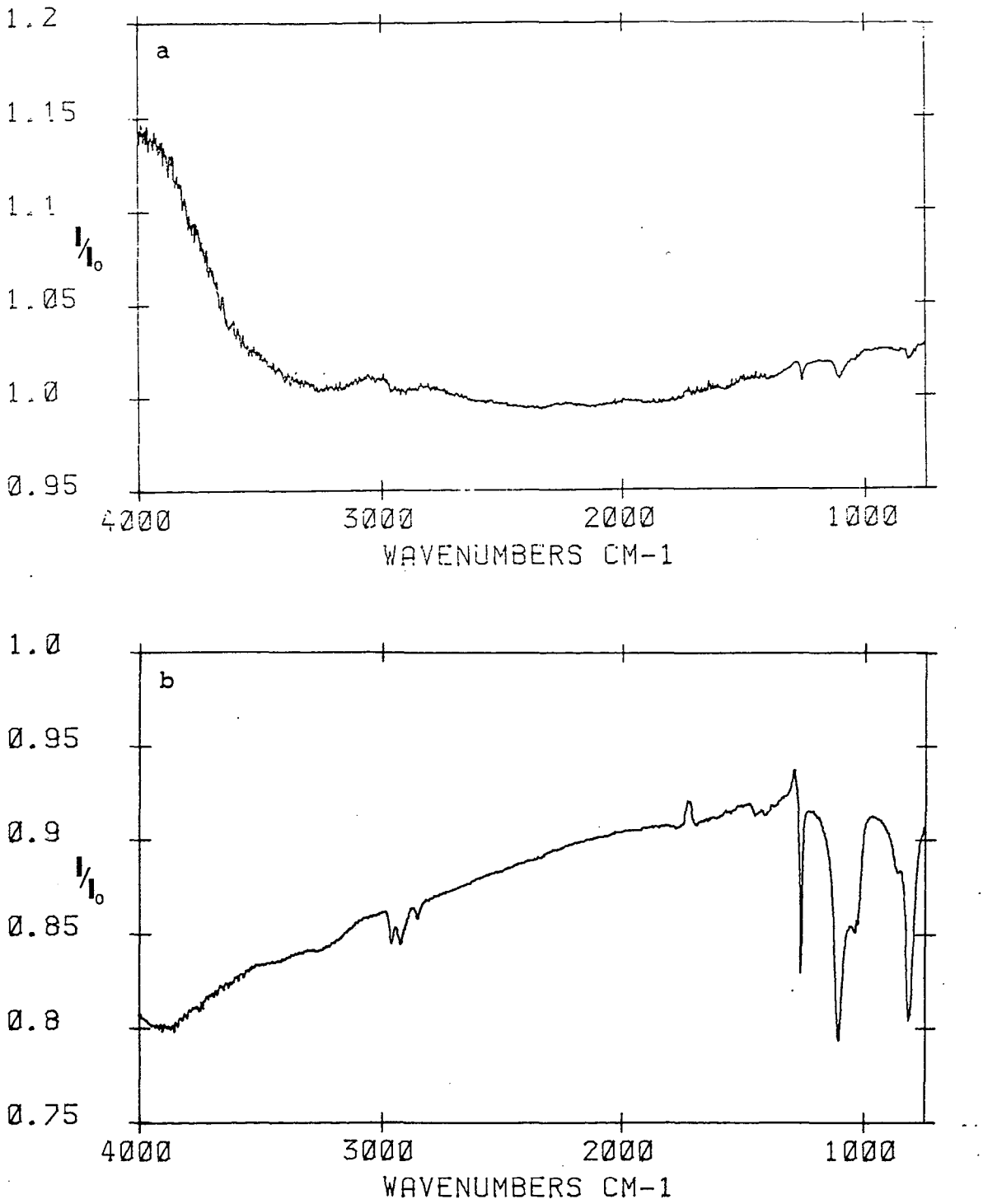


FIG. 8. Spectrum of (a) 5 A and (b) 50 A of silicone oil in a gold-plated copper light pipe. Length: 12.5 cm, ID: 0.3 cm, and 0 to 8 reflections.

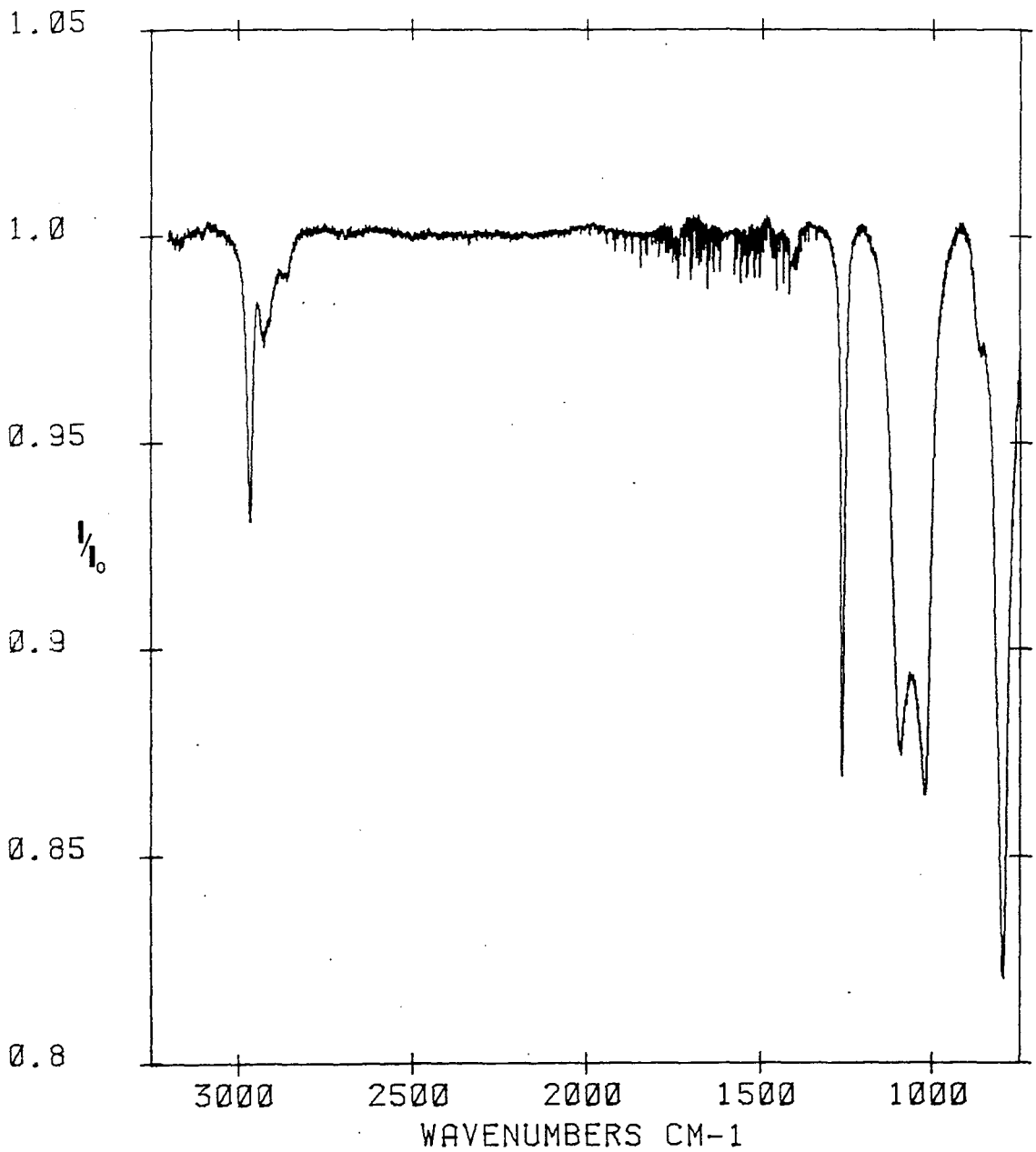


FIG. 9. Spectrum of 10 A of silicone oil in a GMR with 16 reflections.[23]

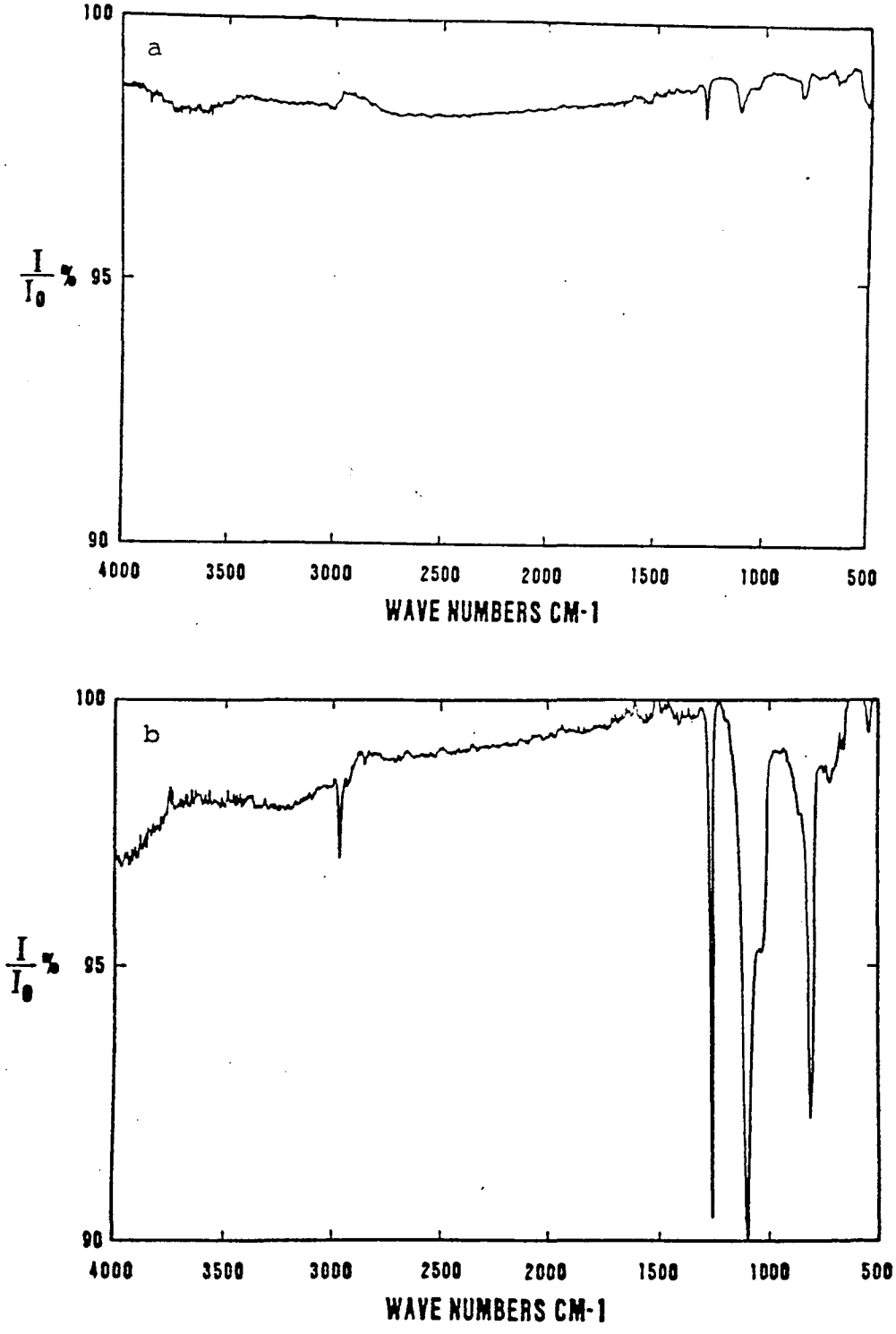


FIG. 10. Spectra of 30 A of silicone oil taken (a) with a single reflection device and (b) with a gold-plated light pipe (length = 18cm, ID = 5mm, 24 reflections).[14]

Unlike conventional spectrometers that relate the intensity to their particular wavenumber with a grating instrument, FTIR spectrometers use a Michelson interferometer to relate the intensity to the pathdifference of the two beams. The resulting intensity that reaches the detector is called an interferogram. The advantages of the FTIR technique is that one usually reaches a higher resolution, a higher throughput, and an easier handling data since the analysis is done by a microcomputer.[16] A disadvantage is that the raw data are no longer usable without the help of a computer. The beamsplitter in Fig. 11 divides the beam in two parts that reflect separatly on the moving mirror and recombine later. Fig. 12 shows a simplified standard version of a Michelson interferometer. In this set-up one can more easily understand the four different spectra and their corresponding interferograms.[16] For the easiest case [Fig. 13(a)] of monochromatic source, the interferogram is just a sinusoidal wave.[12] Fig. 13(c) shows how an actual peak with a finite linewidth results in a damping of the interferogram. In the actual physical case that is shown in Fig. 13(d), the interferogram is centered around zero path difference because every ray combines with its corresponding ray with the same frequency. The information of the spectral adsorption is mostly in the low-intensity wings of the interferogram.[16] To reach the actual data for

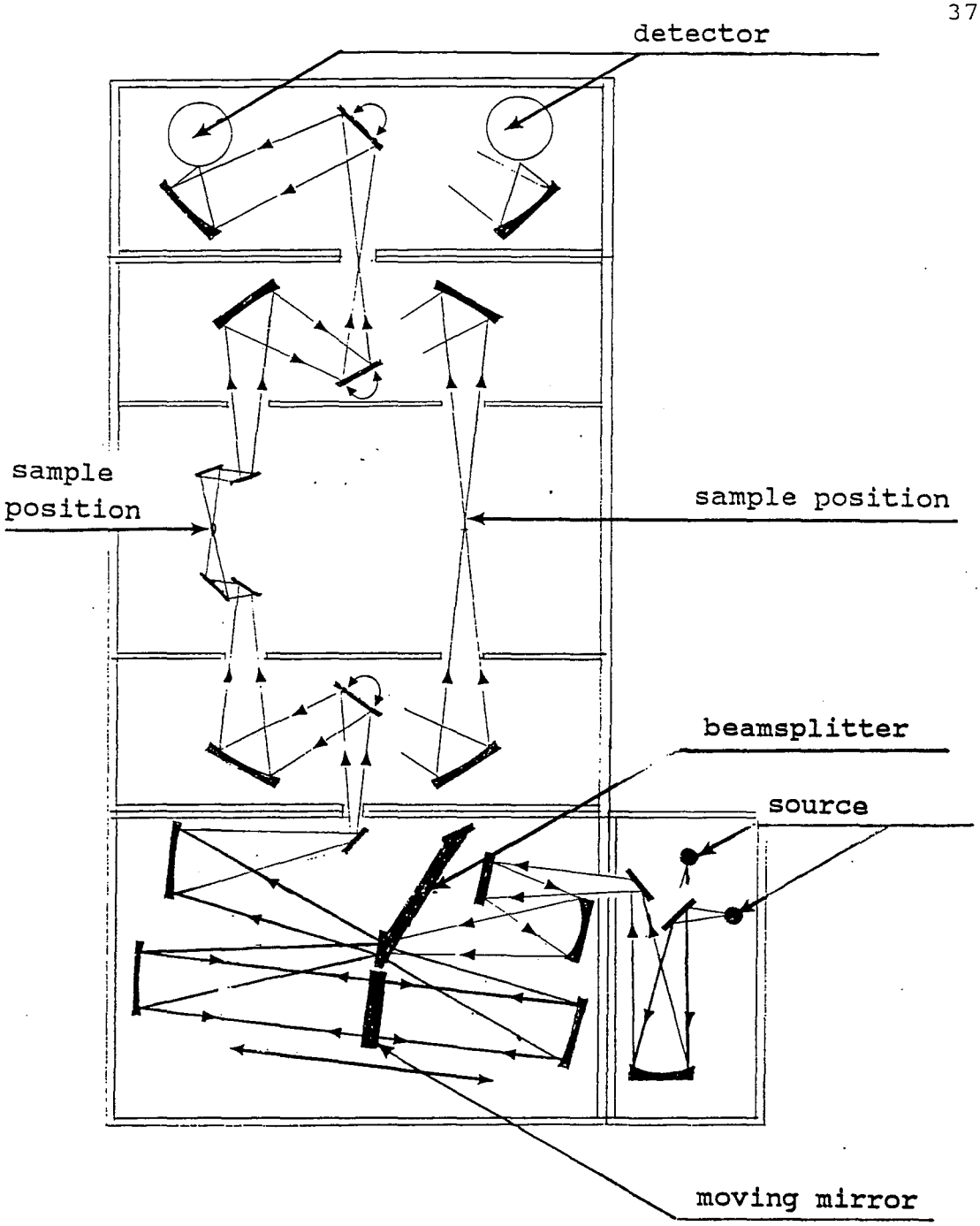


FIG. 11. Optical path in the Bruker 113V FTIR spectrometer.

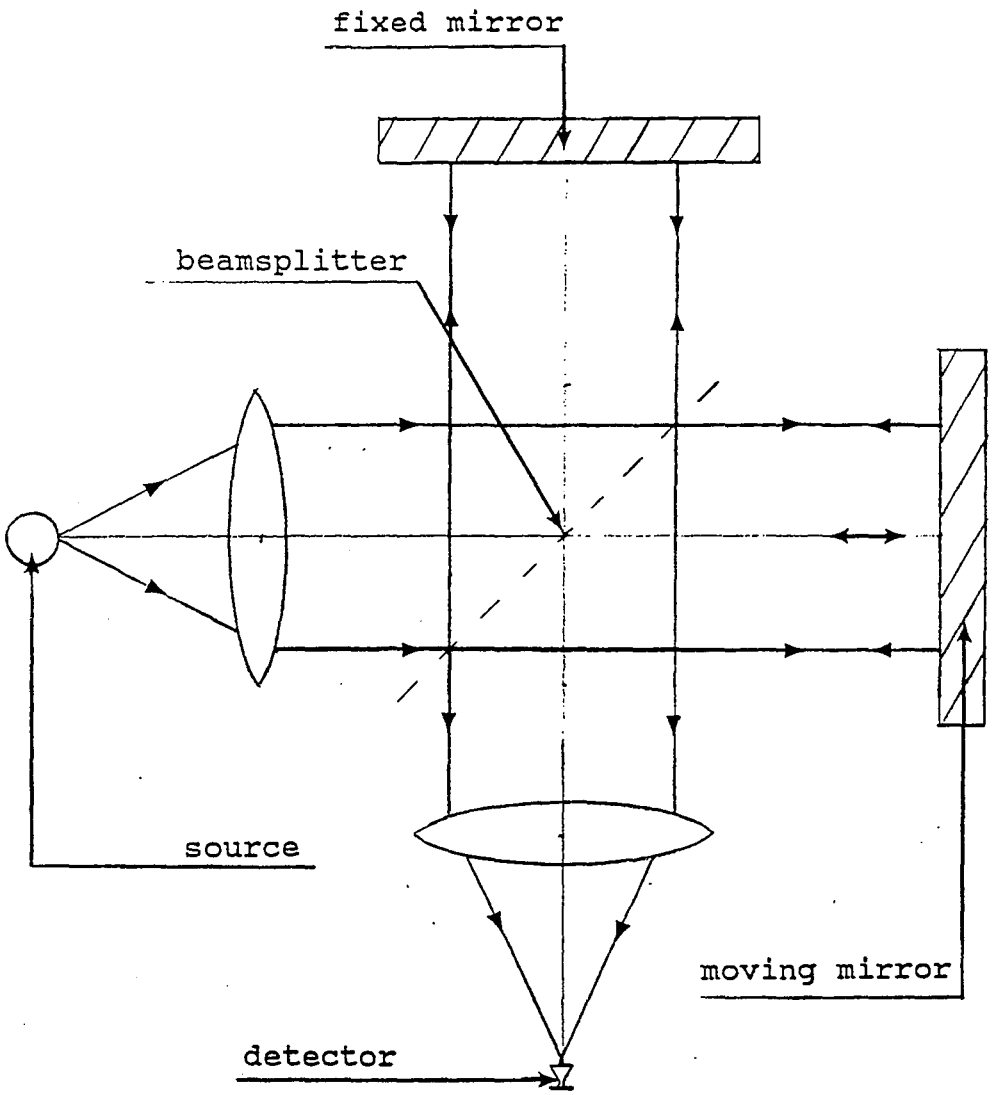


FIG. 12. Simplified schematic of a Michelson interferometer.

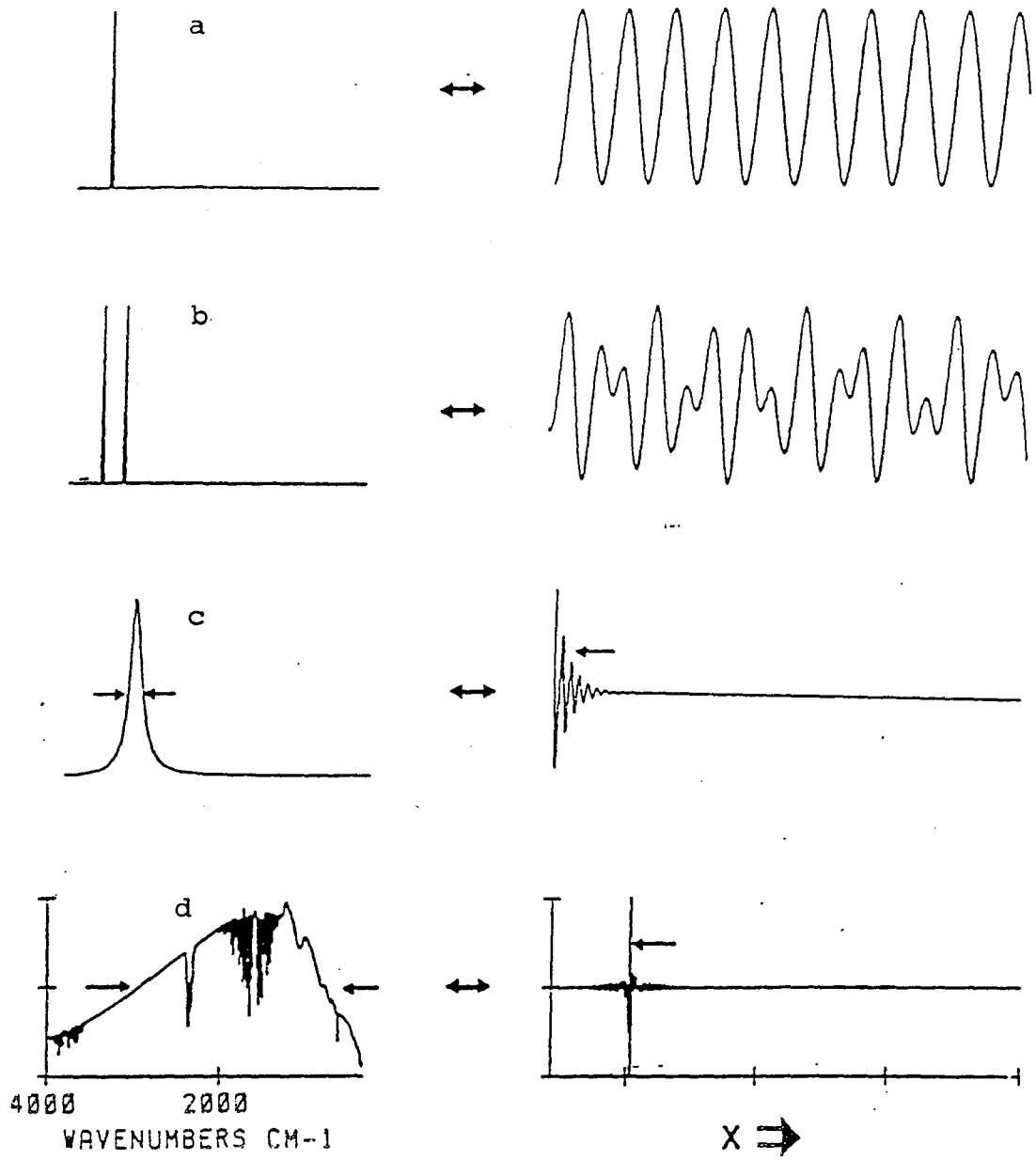


FIG. 13. Graph for four spectra and their interferograms.[16]

a thin film, for example, it is necessary to record two interferograms and ratio them. To regain the spectrum, one needs to Fourier transform the interferogram to get an intensity versus wavenumber graph. Actual data conversion is based on the theory of the Fourier Transformation. Modern computers use a technique called Fast Fourier Transformation to cut computation time and display the data.[16]

The Bruker spectrometer has a natural focus in the center of the sample cell (Fig. 11). The sample chamber is usually pumped down to 2 Torr to avoid water and carbon dioxide bands in the spectra. Generally, the sample chamber is vented with nitrogen to avoid contaminations in the chamber.

Fig. 14 shows how the natural focus is used in the optical set-up. The light pipe is displaced from the optical axis to gain additional path length, which is equal to the length of the light pipe, so that the infrared beam focusses into the opening of the pipe. The image of the focus is then transferred down the tube where the focus of the detector is located. The spherical mirror at the entrance of the pipe does not change the path appreciably, but it increases the angle of incidence so that we get more rays at the maximum of Fig. 7.

The high $T_c$ superconductor and the adsorption measurements of CO on MgO are usually done with different

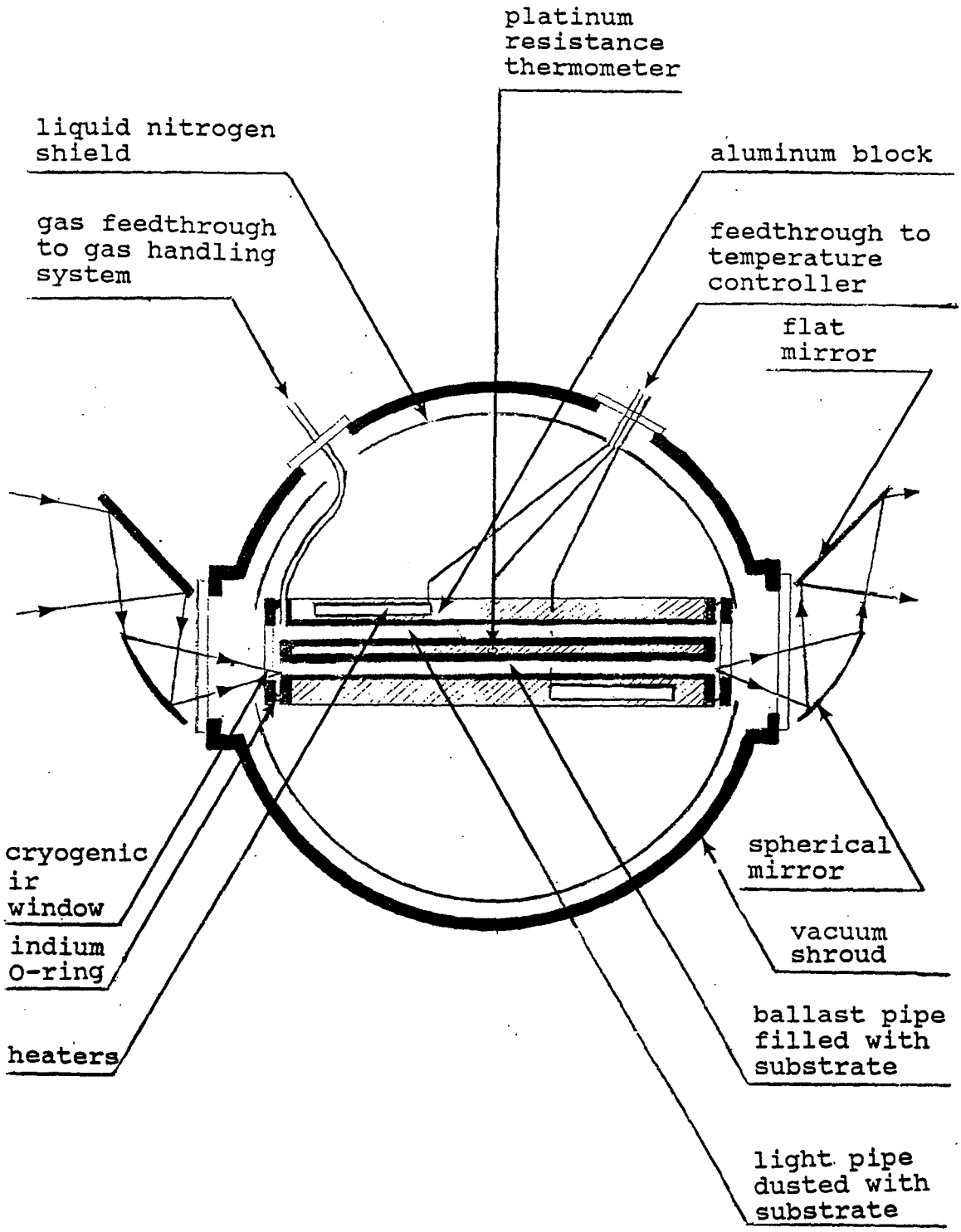


FIG. 14. Optical set-up for the measurements with the dewar and light pipe.

resolutions. Since the change in the HTc superconductor measurements is an overall change in the reflectivity from 500 $cm^{-1}$ to 0 $cm^{-1}$, it is possible to use a resolution of 16 $cm^{-1}$ to speed up the data acquisition and to decrease the noise.[16] For the adsorption of CO on MgO, however, one has to distinguish between the gas peak, which has three-dimensional rotational freedom and is located at 2147 $cm^{-1}$, and the adsorbed peak, which is located at around 2157 $cm^{-1}$ and has a half width of 10 $cm^{-1}$. Since the gas peak shows sharp peaks approximately 4 $cm^{-1}$ apart, it should be distinguishable from the adsorbed peak.[17]

For a usual measurement of CO adsorbed on Mgo we used a common mid ir source, a KBr beamsplitter and a liquid nitrogen detector. For the high Tc superconductor measurements we used a Mercury source, a 3.5 or 23 micron Mylar beamsplitter, and a room-temperature DTGS detector. Appendix C contains a complete listing of all the parameter settings for either measurement.

# CHAPTER III

# LITERATURE REVIEW

The following chapter introduces the reader to the current understanding on both of our initial test experiments. Chap. III Sec. A gives a brief overview of adsorption of gaseous species on surfaces, but focusses on the literature that is relevant for the infrared measurements of CO on MgO. The information on the high $T_c$ superconductor (Chap. III Sec. B) introduces briefly the theory and the coupling mechanisms of common superconductors that are responsible for the energy gap. Finally, several articles on previous measurements of the energy gap are reviewed. Due to the vast number of publications in this field, the review will not be comprehensive and will again focus on the ir measurements.

## A. Carbon Monoxide Adsorbed on Crystals with Sodium Chloride Structure

The presented literature of adsorbates on substrates with NaCl structure can be divided into three parts; thermodynamic information of physisorbed species, structural information of the substrate and the adsorbate (mainly theoretical), and dynamical information of physisorbed and chemisorbed species (mainly ir).

To understand this discussion it is necessary to understand the two types of bonds that can occur between an

adsorbate and a substrate, physisorbed and chemisorbed bonds. The division between physisorbed and chemisorbed bonds is somewhat arbitrary. Physisorption does not transfer an "appreciable" amount of charge between the adsorbate and the substrate, and occurs usually below a binding energy of 0.1 eV per adsorbed molecule, which is equivalent to about 2.4 kcal/mol.[6,10] Physisorption usually originates in a van der Walls[10] interaction, and is a reversible process under standard temperature conditions. Chemisorption, however, does transfer an appreciable amount of charge from the adsorbate to the substrate,[3] and is typically an irreversible process under standard temperature conditions,[24] with binding energies above 0.1 eV per adsorbed molecule.

One way to study these bonds is by a vapor pressure isotherm (VPI). VPIs allow the thermodynamic investigation of gaseous adsorbates on high-surface-area substrates. Next to the coverage, the binding energy is one of the quantities of interest. VPIs can also determine the isosteric heat of adsorption, which is the binding energy per mole. Crowell and Young[33] show that, for an ideal gas, the heat of adsorption depends on the pressure and temperature. For CO adsorbed on MgO, Furuyama[8] *et al.* report VPI at four different temperatures. The equilibrium pressure of a monolayer ($\theta = 1$) at 90.5 K is at approximately 0.5 Torr, while it is around 10 Torr at 102

K. The resulting heat of adsorption is around 3.6 kcal/mol (0.15 eV). Since physisorption is typically weaker than chemisorption, it results in a smaller value of the heat of adsorption, and provides an experimental criteria to determine the kind of adsorption.[6]

A VPI can be used to infer on the structure of an adsorbate on an underlying crystal.[8] Structural calculations (see below) indicate strongly that the adsorption site for the CO molecule is vertical above the $Mg^{++}$ surface ions, which suggests strongly a commensurate overlayer of the adsorbate. For CO on MgO, VPIs provide the primary experimental indication that CO forms a commensurate $\sqrt{2} \times \sqrt{2}$ unit cell with respect to MgO (001) surface structure[8] at monolayer coverage. The measurements show that there are half as many CO molecules as there are Mg or O ions at the surface at monolayer coverage. Together with the structural calculation, the experimental result suggests strongly the $\sqrt{2} \times \sqrt{2}$ unit cell. There can be no denser commensurate layer (e.g., 1 x 1 ) because the van der Walls radius of a CO molecule is larger than the distance between two Mg or two O ions on the MgO (001) surface.[8]

Homogeneity and cleanliness of a substrate are also determined with VPI in an indirect way. Substrates that are contaminated with impurities in the lattice do not show a reversible adsorption or at least a much higher isosteric

heat of adsorption while a contaminated substrate surface does not show adsorption at all.[5] This is also confirmed by model calculation[3], which shows that there is an irreversible heat of adsorption between 10 and 15 kcal/mol for MgO that was doped with metals such as Li, Na, Cu, Al, and Zn. The homogeneity of a substrate, however, is determined by a sharp bending of the step in a $n_{ads}$ versus $P_f$ diagram. For a homogeneous substrate, the step will be sharper than for a heterogeneous substrate.[20]

For the measurements of CO on MgO, VPI[8] and electron micrograph[24] measurements show that MgO forms cubic microcrystals with a sodium chloride structure that have mostly (001) surfaces exposed.[24] Depending on the preparation,[26] the surface[5,26] area and the particle size can vary from below $10m^2/g$ up to 200 $m^2/g$, and the crystallite size can vary from a micron to tens of Angstroms.

Model calculations using a classical approach confirm the conclusions drawn from the VPI and show that the preferred position for CO on MgO is vertical above every other Mg ion on the (001) surface.[3,6,10] There is, however, disagreement between Dorvesi *et al.*[6] and Colbourn *et al.*[3] about the type of adsorption and the heat of adsorption. While Colbourn *et al.* predict chemisorption for CO on MgO with 9 kcal/mol, Dorvesi *et al.* predict physisorption with a heat of adsorption between 4.1 kcal/mol and 3.3 kcal/mol. Both find the preferred position to be vertical to the

surface and above the Mg ions. In agreement with Dorvesi *et al.*, VPI and ir measurements do, however, show that CO physisorbes on MgO (001) with a heat of adsorption of 3.6 kcal/mol.[8] The differences in the calculations might be originated in assumptions and approximations. The binding energy is the difference of several energy terms that are large compared with the final binding energy. A small relative error in one approximation could, therefore, produce a relatively large error in the final result for the binding energy.

Neither calculation can determine if the bond is made through the C or the O atom of CO. The heat of adsorption, electron transfer, electron density, and stretching of CO are too close to determine the preferred orientation.[3,6] A ferromagnetic state would occur if the dipole moments of CO molecules were aligned, and an antiferromagnetic state would have alternating dipole moments. The difference of the vibrational frequency of the ferromagnetic state (all CO molecules aligned) and the antiferromagnetic state (alternating C-down O-down molecules) will be closer together than the halfwidth of the expected vibrational stretch mode.[10] To solve that problem there has been some effort in our group to measure the structure directly using X-ray diffraction, since the ir measurements will not be able to address this problem.

Colbourn *et al.*[3] calculate, in the same manner as for the (001) surface, the binding energy for chemisorbed CO on corners and steps to be 15 kcal/mol and 9.4 kcal/mol. Even though this calculation has not been carefully tested by experiments, there are two conflicting indications. An analogy to the ir measurements of CO on NaCl would predict that CO physisorbs with a far lower heat of adsorption,[34] while the ir measurements of CO on chemically treated MgO does show chemisorption with a heat of adsorption that is comparable to the one calculated by Zecchina *et al.*[11]

Measurements of the dynamics of adsorbed species on crystalline substrates have been widely used to study the bonds between the adsorbate and the substrate as well as between the adsorbate itself.[9,10,11,24,25,34] He scattering, EELS, INS, and infrared probes can excite the vibrational modes of the adsorbed species. In the case of CO adsorbed on crystals with NaCl structure, the predominate excited mode is a stretch mode in the CO molecule.[10,24,34] The location and the appearance of the ir mode compared to the gas spectrum contains the information about the binding energy of the adsorbed molecule.[10] The vibrational mode is altered because the intermolecular force between the C and the O in an adsorbed CO molecule is larger than in gaseous CO. Gevirzman *et al.*[10] used a classical electrostatic approach to calculate the location and orientation of CO on NaBr, NaI, and NaCl and to calculate the shift in the vibrational

stretch mode. The comparison with their own ir spectra shows remarkable consistency for the position of the peak as well as for the shift due to increasing coverage. The experimental absorption peak is displaced from the gas peak (2144 $cm^{-1}$) around +14 $cm^{-1}$ for low coverage for all three crystals and drops to +10 $cm^{-1}$ for monolayer coverage. The calculated shifts are +9 $cm^{-1}$ and simulate the environment of monolayer coverage. This suggests that the ir absorption for CO on MgO should also be displaced by about 14 $cm^{-1}$ and drop to 10 $cm^{-1}$, because of the identical crystal structure. There is, however, a slight difference between the sodium halogens and MgO. MgO will form $Mg^{++}$ and $O^{-}$, which leads to a different strength in the bonds because Na donates only one electron in sodium halides. Qualitatively this has been confirmed with the only available publication of ir measurements for CO on MgO. Zecchina *et al.*[24] measure the ir absorption peak for CO adsorbed on MgO at 2152 $cm^{-1}$ at monolayer coverage. This is a displacement of about 8 $cm^{-1}$ from the gas peak. They also report the spectra for other alkali metal halides, including NaCl and NaI, which show slightly higher wavenumbers than Gevirzman's. The results of Zecchina *et al.* can be summarized as follows. CO on the (001) surface of MgO shows predominant physisorption with an absorption peak at 2152 $cm^{-1}$ for $\Theta$ = 1. At lower coverage ($\Theta \rightarrow 0$) the spectrum shows a doublet at 2170-2164 $cm^{-1}$ and 2151 $cm^{-1}$. Isotopically labeled CO in

a mixture of 10:90 of $C^{12}$:$C^{13}$, however, shows only one peak for $C^{12}$ at low coverage that is placed at 2148 $cm^{-1}$. The doublet is unique to CO adsorbed on MgO, but was not further investigated. An additional weak peak at 2100 $cm^{-1}$ is associated with natural occurring $C^{13}$. There is also a weak feature of irreversible species of chemisorbed CO in the spectrum, which did not disappear during a pumpout while all other peaks did. The interaction of CO molecules is discussed in a general sense with all other alkali metal halides, since it apparently does not show any anomalies. The CO interaction of isotopically labeled CO shows that a coupling only takes place if the adsorbed molecules have the same vibrational frequency. $C^{12}$ does not couple with $C^{13}$ in a 10:90 mixture, and the absorption peak of $C^{12}$ does not shift to lower wavenumber as the coverage increases. The report shows that the modified Hammaker equation allows good predictions of the spectral shift with increasing coverage.

$$(\omega/\omega_0) = 1 + \frac{\Theta\ \alpha_e\ \Sigma_o}{1 + \Theta\ \alpha_,\ \Sigma_o}\ , \qquad (6)$$

where $\omega$ is the observed frequency, $\omega_0$ is the vibrational frequency of an isolated CO molecule on the surface, $\Theta$ is the coverage, $\alpha_e$ is the static polarizability, $\alpha_,$ is the dynamic polarizability, and $\Sigma_o$ is the dipole sum.

Zecchina[34] published an earlier paper on the static and dynamics of CO on sintered NaCl films. The paper covers the same topics, but also covers the spectrum of CO adsorbed on edges and corners and for several isotope concentrations. The paper is probably the most comprehensive ir work of CO physisorbed on NaCl. The absorption peak for $C^{12}$ is at 2157 $cm^{-1}$ and shifts to 2162 $cm^{-1}$ as the coverage approaches zero. The vibrational peak of the natural isotope $C^{13}$ is much weaker and located at 2107 $cm^{-1}$. The effect of an 8:92 mixture is similar to the one with MgO. The intensity for different mixtures at a given pressure scale very well so that an equal heat of adsorption can be assumed. Spectra of CO on different surface area substrates tend to indicate that lower surface substrates show fewer peaks due to defects. The main peak at 2157 $cm^{-1}$ is, however, much weaker since there are less CO molecules per mass of substrate. The intensity of the vibrational mode for CO adsorbed on steps shows up at 2175 $cm^{-1}$ and reaches its maximum long before the intensity of the absorption peak for the (001) surface reaches its maximum. The heat of adsorption for the steps seems, therefore, higher than for the (001) surface. The molecules on the steps do not show a shift due to coverage, because they cannot couple dynamically with CO adsorbed on the (001) surface, which are at different vibrational frequencies. The shift due to the coverage at the (001)

surface is again explained with the modified Hammaker equation and is to about 2161 $cm^{-1}$.

In the case of an MgO substrate that has many defects and corners, CO will, however, chemisorb. For chemisorption it is believed that CO will form larger molecules, such as bridge and ring molecules with several CO bound together.[9,11] Spectra of CO on MgO with a surface area of 250 $m^2/g$ have been measured,[11] and the vibrational absorption bands appear between 1000 $cm^{-1}$ and 2000 $cm^{-1}$.

There is one fact worth mentioning that cannot be determined by any measurement on powdered samples. The orientation of the molecule on the substrate cannot be investigated due to a random order of the powdered substrate. Richardson *et al.* measured that CO adsorbs vertical on (001) NaCl single crystals by measuring the absorption of a polarized ir beam. The result was that only a beam polarized perpendicular to the (001) surface of NaCl could excite the adsorbed CO molecules. This is strong evidence for a vertical adsorption of CO on NaCl and also, by analogy, on MgO. Unfortunately the technique is only applicable for materials that are ir transparent and not for MgO.

## B. High $T_c$ Superconductors

Historically, there have been three major techniques to test if a material is superconducting. The resistance

of a superconductor should drop to zero, it should expel magnetic fields (Meissner effect), and it should show an energy gap at the Fermi energy. In this review, I will focus on the measurements of the energy gap that can be measured with tunneling or infrared spectroscopy because those measurements allow a quantitative comparison with predictions of the BCS theory. The BCS theory is developed for low-temperature superconductors and should not be applicable for high $T_c$ superconductors because the superconductivity is originated in an electron-electron interaction.

The BCS theory explains superconductivity in the following way. Two electrons can form a Cooper pair; that means they can be bound by a phonon exchange to reach a lower overall energy. Because of energetic reasons, it will be most likely that two electrons with opposite crystal momenta and close to the Fermi level will form a Cooper pair. Fig. 15(a) shows the probability of occupying a state with energy E. At 0 K, the probability of states for a superconductor looks like the probability of states of a normal conductor at higher temperature. The density of states, however, shows a gap because electrons below and above the Fermi level have an additional energy due to the exchange of a phonon. Fig. 15(b) shows the density of states for a superconductor. The BCS theory predicts the size of the energy gap to be

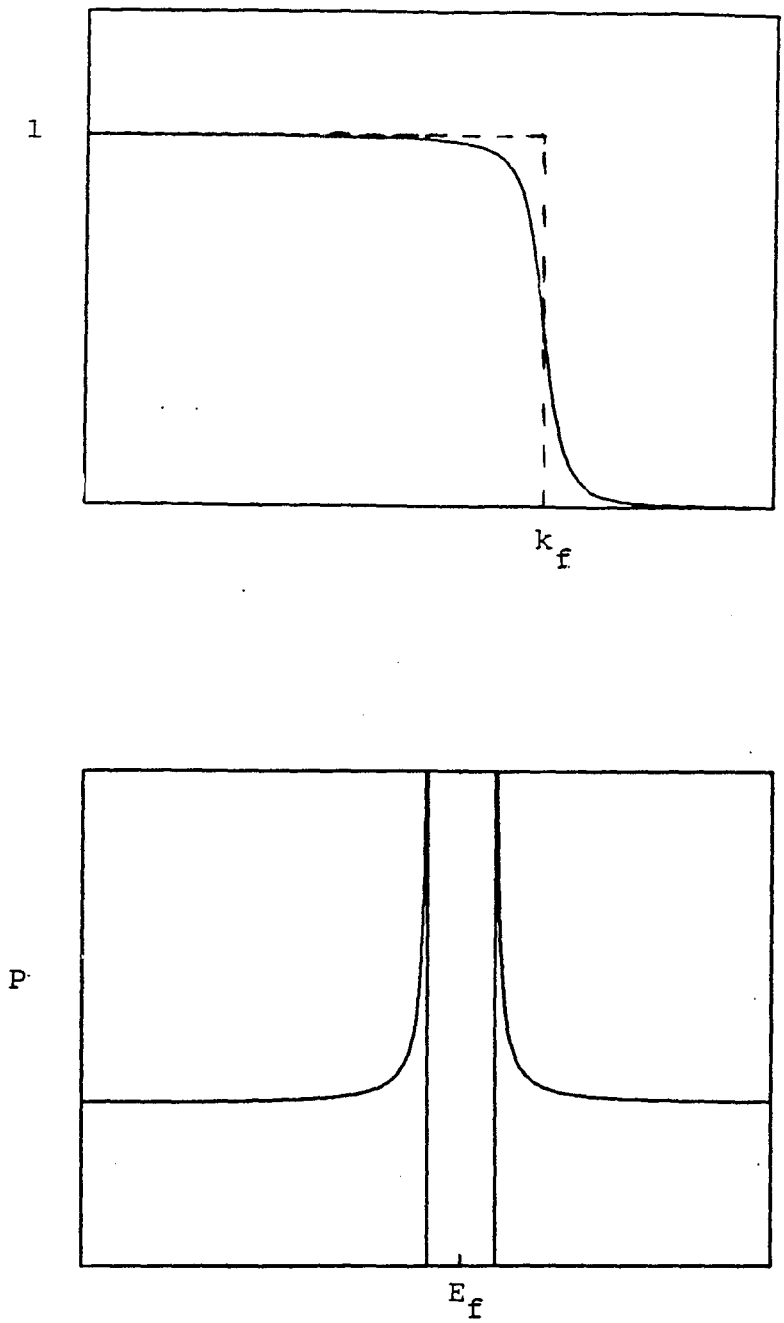


FIG. 15. (a) Probability of states for a high $T_c$ superconductor at 0 K (solid line) and for a common material (dashed line), and (b) the resulting density of states for the high $T_c$ superconductor.

$$2\ E_g\ /\ k_B\ T_c = 3.5,$$

while for an electromagnetic wave the excitation energy gap is given as $E_g = h\omega$. This yields to a cutoff wavenumber of

$$1/\lambda\ = (3.5\ k_B\ T_c)/(2\ h).$$

Even though there is no reason, a priori, why the new high $T_c$ superconductors should follow this relation or should have an energy gap at all, they all show an energy gap in the right order of magnitude. The measurements of the energy gap, however, need to be explained by any theory that describes the new high $T_c$ superconductors and their features.

There are two points worth mentioning. First the energy gap in high $T_c$ and normal superconductors are of completely different origin than energy gaps in semiconductors or insulators. For superconductors the energy gap is originated in an electron-electron interaction by a lattice vibration (phonon), while the gaps of semiconductors or insulators are originated in an electron-lattice interaction which creates bands and gaps. The electron-electron interaction in superconductors will vanish when the temperature increases above the critical temperature because the lattice will vibrate and destroy the electron-electron induced phonons.

The reports in the literature about the size of the energy gap vary substantially. There are reports for $(2\ E_g)/(k_B\ T_c)$ that vary between 1.3 and as high as 8.[7,18,19,26,27,29]

Earlier reports on sintered powders seem to indicate that the energy gap is smaller than the prediction for the BCS theory,[19,27,32] while newer reports, especially on single crystals, seem to show bigger energy gaps.[7,18,28] $YBa_2Cu_3O_7$, for example, show a ratio[19] for $(2\ E_g)/(k_B\ T_c)$ between 1.3 and 2.7 for measurements on sintered powder, while the same group reports a ratio of 8 for a single crystal.[28] The differences in those results might originate in a different sample preparation of the superconductor, while the difference between the single crystal measurements and the sintered powder indicate highly anisotropic substrates. There is, for example, no superconductivity and a much smaller energy gap for single crystal $YBa_2Cu_3O_7$ if it is measured perpendicular to the CuO planes, while both are well defined parallel to the CuO planes.[27] However, all the literature consistently reports that the energy gap increases if the temperature decreases.[1,7,18,19,27,28,32] There is also consistency in that the spectrum does not simply show an increase in the reflectivity, but has some structure due to optical phonon adsorption.[1]

For our measurements on $YBa_2Cu_3O_7$ we should expect an increase in the reflectivity in the far ir if the sample is cooled below its critical temperature. The reflectivity should increase as we decrease the sample temperature.

# CHAPTER IV

# SPECTRA TAKEN WITH THE METAL LIGHT PIPE AND DISCUSSION

In the experimental design, the light pipe is used as a light guide similar to a fiber optics guide. The incoming rays reflect off a specular surface, and the focal point is transferred from the entrance of the pipe to the exit. The light pipe should, in theory, enhance the signal by the numbers of reflections and leave the noise approximately the same. Fig. 10(a) and 10(b) show spectra of a 30 A thick layer of silicone oil, one taken with a Cassagrenian optics and the light pipe with 25 reflections, and one taken with a single external reflection device. The enhancement due to the light pipe is obvious, and the small drift of the baseline compared to the enhancement is clearly visible. The throughput of the light pipe depends strongly on the light pipe material, the reflecting surface, and the optics one uses.

For our experiments we decided against the use of a Cassagrenian optics and used a highly polished copper light pipe instead of a gold-plated light pipe. Earlier attempts with a gold-plated pipe did not show a noticeable increase in the throughput, but did prevent the light pipe from oxidation and corrosion. Copper also does not seem to be the best material for the light pipe because it tends to anneal and soften after several bakeouts. Titanium may be

a good choice since it is relatively easy to machine and can stand bakeouts very well. Also, titanium is much easier to plate than stainless steel, which would otherwise be a very good light pipe material.

Fig. 7 shows the mean square electric field parallel to the surface as a function of the incident angle. As one can see, it is most favorable to reach an angle between 60 and 88 degrees because the electric field just outside the reflecting surface is enhanced by a factor of 3.5. Because of that and the high overall throughput (around 75%), we chose to use the optical setup shown in Fig. 14 instead of the Cassagrenian optics. For the meridional rays (Fig. 16) with an incident angle, one gets $N=(L/d)\tan(\Theta)$, where N is the total number of reflections and L is the length of the pipe and d is the inside diameter of the pipe. Following Hansen's *et al.* notation, the angle $\Theta$ is the angle between the light pipe axis and the incoming ray, while $\Theta_1$ will be used as the angle between the surface normal and the incoming ray. In our case, with a 10 cm long pipe, and an inside diameter of 3 mm, we reach a maximum of 7 reflections for an incident angle between 80 and 90 degrees. Fig. 16 shows a sketch for the incoming meridional rays of angle $\Theta$. For the basic theory that will follow, skew rays will not be taken into account and only meridional rays will be discussed. Skew rays follow a

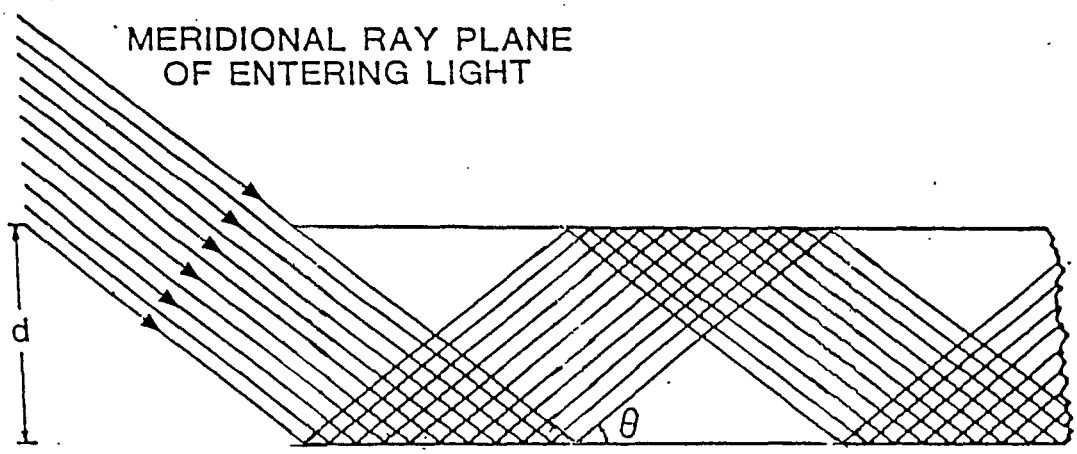


FIG. 16. Schematic of how a meridional ray penetrates through the light pipe.[14]

screw path in the light pipe and might exceed the maximum in the graph in Fig. 7 and are, therefore, difficult to treat. The Poynting vector for an electromagnetic wave is given by the following equation.

$$S_{ave} = E \times H^{*} \quad ( \text{MKSA units} ). \tag{7}$$

The Poynting vector gives the energy that passes through a unit area per second in the direction $E \times H$. All physical measurements require a time far beyond the period of the light, so that the only quantity of interest is the time average of the Poynting vector.

$$S_{ave} = 1/2 \; Re \; ( E \times H^{*} ). \tag{8}$$

Some frequencies of the energy are absorbed and dissipated as heat, while other pass through the light pipe undisturbed. The rate of absorption is given by the negative gradient of the average of the Poynting vector.

$$-\nabla \cdot S_{ave} = - 1/2 \; Re \; ( \nabla \; E \times H^{*} ), \tag{9}$$

$$= - 1/2 \; Re \; ( H^{*} \; \nabla \times E - E \; \nabla \times H^{*} ), \tag{10}$$

$$= - 1/2 \; \sigma \; \langle E^{2} \rangle, \tag{11}$$

where $\sigma$ is the product of n, k, and $\nu$, and n and k are the real and the imaginary part of the complex index of refraction, while $\nu$ is the frequency of the light.

If we further define two quantities A and $\eta(\Theta)$, where A is the energy lost per reflection and $\eta(\Theta)$ is the number of reflections per unit length, we can write

$$I/I_{o} = ( 1 - A )^{\eta(\Theta)L}, \tag{12}$$

where I is the measured intensity at the detector, $I_0$ is the intensity at the detector without the sample, and L is the length of the pipe. Since one usually uses thin coatings, one can assume that $A << 1$ (it will be mentioned in the later sections that this assumption is not always valid) and expand it into a Taylor Series. The polynomial expansion leads to an exponential expression for the transmittance.

$$I/I_0 = exp\ (\ -\eta AL\ ). \tag{13}$$

If we define, furthermore, the absorption coefficient $\alpha = \eta A$, we get the final result for the intensity ratio

$$I/I_0 = exp\ (\ -\alpha L\ ). \tag{14}$$

Following Eq. (11), the rate of adsorption during a reflection can be defined as the ratio of the mean square electric field at that point and the mean square electric field just before it penetrated into the sample. Since it is possible that the light pipe is not completely illuminated with the ir beam (see Fig. 16), we have to divide the ratio also by $sin\theta$ to get the correct "filling factor,"

$$A = < E_2>/<E^2>_0\ (sin\theta)^{-1}. \tag{15}$$

Using the result of the previous discussion $\eta = \tan(\theta)/d$ and $\alpha = \eta A$ we get

$$\alpha = c < E^2>/ < E^2>_0\ (d\ cos\theta)^{-1}, \tag{16}$$

where c is a constant just depending on the material of the tube and the coating in the tube. For highly reflecting

materials such as copper or gold, the constant has been determined and Eq. (16) can be written in its spacial components.

$$< E_2>/<E^2>_o = 4\ sin^2\Theta_1, \tag{17}$$

$$< E_2>_x/<E^2>_o = 4/(n^2+ k^2), \tag{18}$$

$$< E_2>/<E^2>_o = 4\ cos^2\Theta_1/(n^2+ k^2). \tag{19}$$

Eqs. (17,18,19) are valid as long as the $\Theta_1$ does not exceed the pseudo-Brewster angle, which is defined to be the maximum of the graph in Fig. 7. As usual, z is defined to be normal to the surface of the pipe while x is the projection of a ray on the pipe surface. For good reflecting metals, and if $\Theta_1 < \Theta_B$, we will reduce Eqs. (17,18,19) to just one since n and k are large. Using the previous results [Eqs. (15),(17),(18),(19)] and that $\cos(\Theta) = \sin(\Theta_1)$, we obtain for $\alpha$,

$$\alpha_{\parallel} = 0, \tag{20}$$

$$\alpha_{\perp} = c' \sin \Theta_1. \tag{21}$$

Fig. 7 shows a plot of the parallel component of the mean square electric field. Until the graph gets close to the pseudo-Brewster angle, it is described well by Eq. (17). As previously mentioned, it is preferable to design the optics so that the reflections are near grazing angles.

Usually $\alpha$ has three components; the sample itself, the metal light pipe, and scattering.

$$\alpha = \alpha_s + \alpha_m + \alpha_{sc} \tag{22}$$

I will discuss the effect of the sample and scattering in the next two sections. The effect of the light pipe is neglected here since it is very small for highly reflecting materials, does not change much with wavelength, and is ratioed out of the final spectrum.

## A. The Effect of Thin Coatings on the Metal Light Pipe

In the case of a thin coating, the theory described is valid. One can assume that the absorbtivity of the coating is just added to the spectrum because $\alpha$ is small, as assumed in the previous derivation. If one takes the clean light pipe as a reference spectrum, the only change will be in the added coating. Fig. 8(a) and 8(b) show two spectra of a 5 A silicone film and a 50 A silicone film. The spectra scale within 10% for ratio of the absorbance divided by the thickness of the layer and only adsorption peaks show up, which are the vibrational excitation of silicone oil.

## B. The Effect of Powders on the Light Pipe

The assumptions of the previous section require a thorough justification for the use of powders in the light pipe. First, because of the particle size, there will be an appreciable amount of absorption due to scattering from the substrate, since $\alpha_{sc}$ can no longer be neglected; second

the phase and intensity changes can no longer be assumed to be small. Finally, for experimental reasons, the layer usually exceeds 0.5 microns because one wants a strong absorption signal from the gas on the substrate. Thus, one can no longer assume that $\langle E_z \rangle / \langle E_z \rangle_o$ stays the same for a coated light pipe and for a clean light pipe and that the pseudo-Brewster angle remains the same, since the assumption of a one-phase system is no longer valid.

Since there is no theory yet that describes a three-phase system (adsorbate on a powdered substrate on the light pipe material) where one phase is a powder, we will just discuss our data and try to explain their spectra.

The particle size is sometimes larger than the coating that should be placed in the light pipe. The thickness of the layer is that calculated by assuming infinitesimal small particles that would form a uniform layer. For example, in the case of graphite, a 0.2 micron layer does not mean a complete coating of the light pipe with particles 0.2 micron in size, but rather that 10% of the light pipe is coated with graphite particles that are 2 microns and 90% is not coated.

Usually the adsorbent is mixed with a volatile solvent, such as acetone or methanol, and then placed in the light pipe to get the powder to stick on the inside walls. The solvent evaporates and a uniform layer of the adsorbent remains. For the actual simultaneous ir and VPI

measurements, the light pipe is baked at 500° C to drive off remaining residues.

All the spectra of powders in the light pipe show the same kind of behavior and adsorb the ir beam strongly at high wavenumbers and less at low wavenumbers. Fig. 17 shows the spectrum of a 0.2 micron layer of graphite in the light pipe and Fig. 18(a) and (b) and Fig. 19(a) and (b) show them for two particle sizes of $Al_2O_3$ and MgO. The throughput between 4000 and 1750 wavenumbers per cm is very low. The region of interest for the measurement of adsorbed CO is between 2250 $cm^{-1}$ and 1750 $cm^{-1}$, which is in the region that shows low throughput for coatings thicker than 1 micron. As expected, graphite adsorbs the strongest while $Al_2O_3$ adsorbs the least. This can be explained with the high conductivity of graphite (around $10^5$ mohs/meter), which gives a penetration depth of the order of a few hundred Angstrom for the ir, while MgO is an insulator and has a penetration depth of several microns. Table 1 shows the calculations for the penetration depth of graphite, MgO, Cu, and Au for the ir region. Therefore, a coating in the submicron range of two micron sized graphite is opaque in the ir and does not allow good data acquisition because the noise level will be too high and the strong gas phase spectrum will overlay the weak adsorbed spectrum.

Fig. 19(b) shows the spectra for three different

TABLE 1. Penetration depth for copper, gold, graphite, and magnesium oxide.

| Substrate | Penetration depth in the ir in A |
|---|---|
| graphite | 200 |
| MgO | 35000 |
| copper | 10 |
| gold | 10 |

thicknesses for Puratonic MgO, and Fig. 19(a) shows the spectra for MgO that was prepared by Dr. J. R. Dennison and Teresa Burns in our lab by burning Mg ribbon in a controlled oxygen nitrogen environment.[5,21] Both kinds of MgO show comparable crystallite sizes in the X-ray diffraction (around 320 A) but show a different absorption for the ir beam. The preparation of the material suggests a different physical particle size for the smoke and the Puratonic MgO because the smoke settled much faster in a methanol mixture. This suggests that a major part of the adsorption is due to scattering. An investigation of the two powders with an electron micrograph would answer this question definitely and is planned. The general trend of the spectrum is probably caused by scattering and adsorption, while the peak at 800 $cm^{-1}$ is due to an

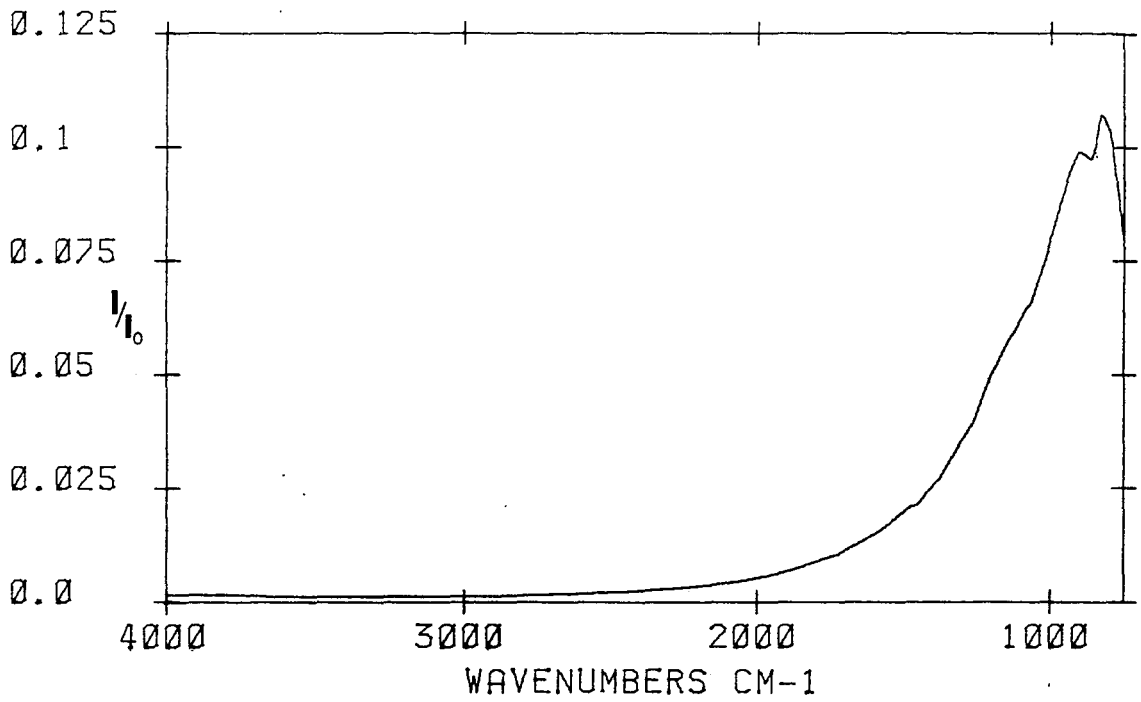


FIG. 17. Spectrum of 0.2 microns of graphite in a copper light pipe.

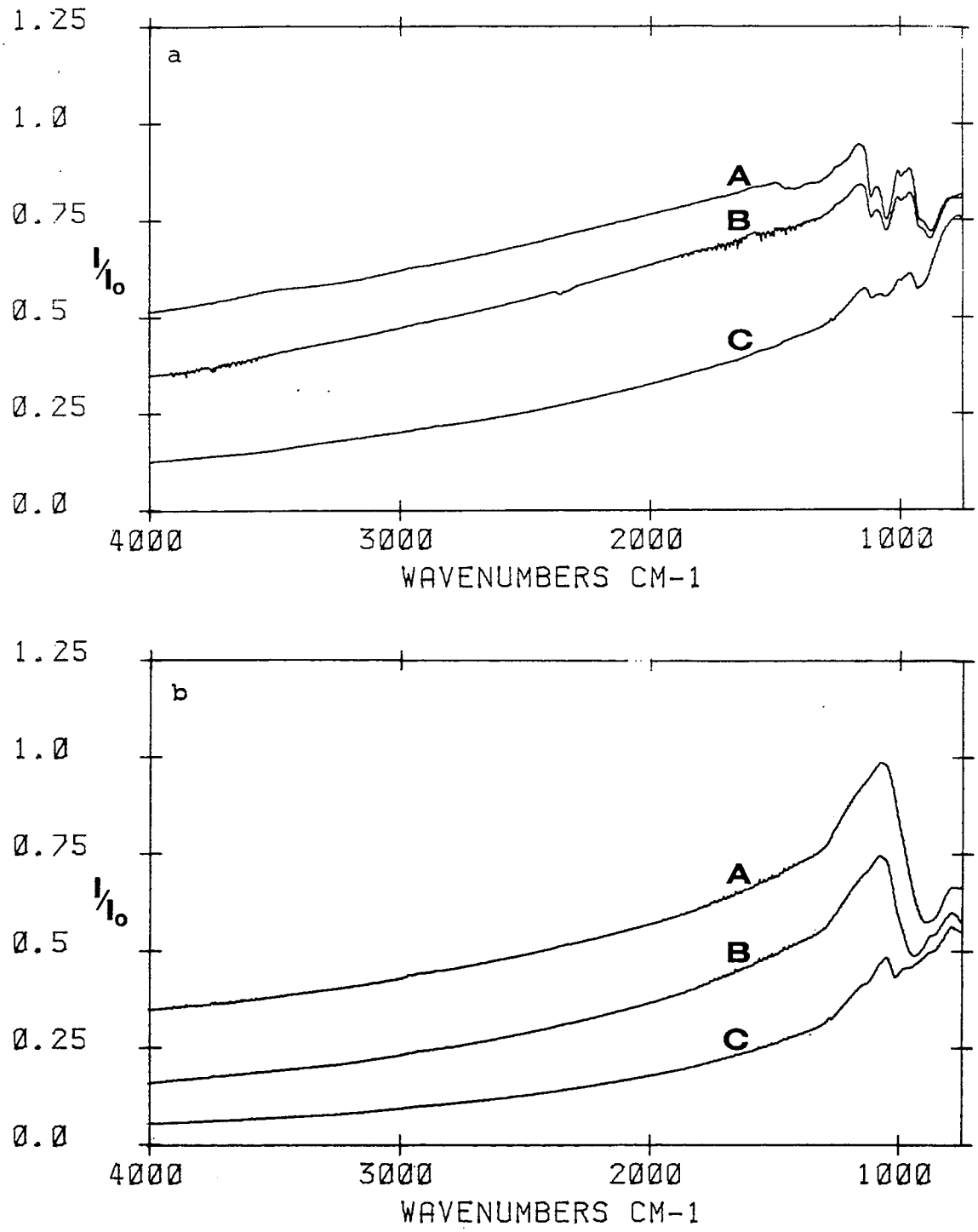


FIG. 18. Spectra of (A) 0.25, (B) 0.5, and (C) 1 microns of (a) 0.05 micron-sized $Al_2O_3$ and (b) 0.3 micron-sized $Al_2O_3$ in a copper light pipe.

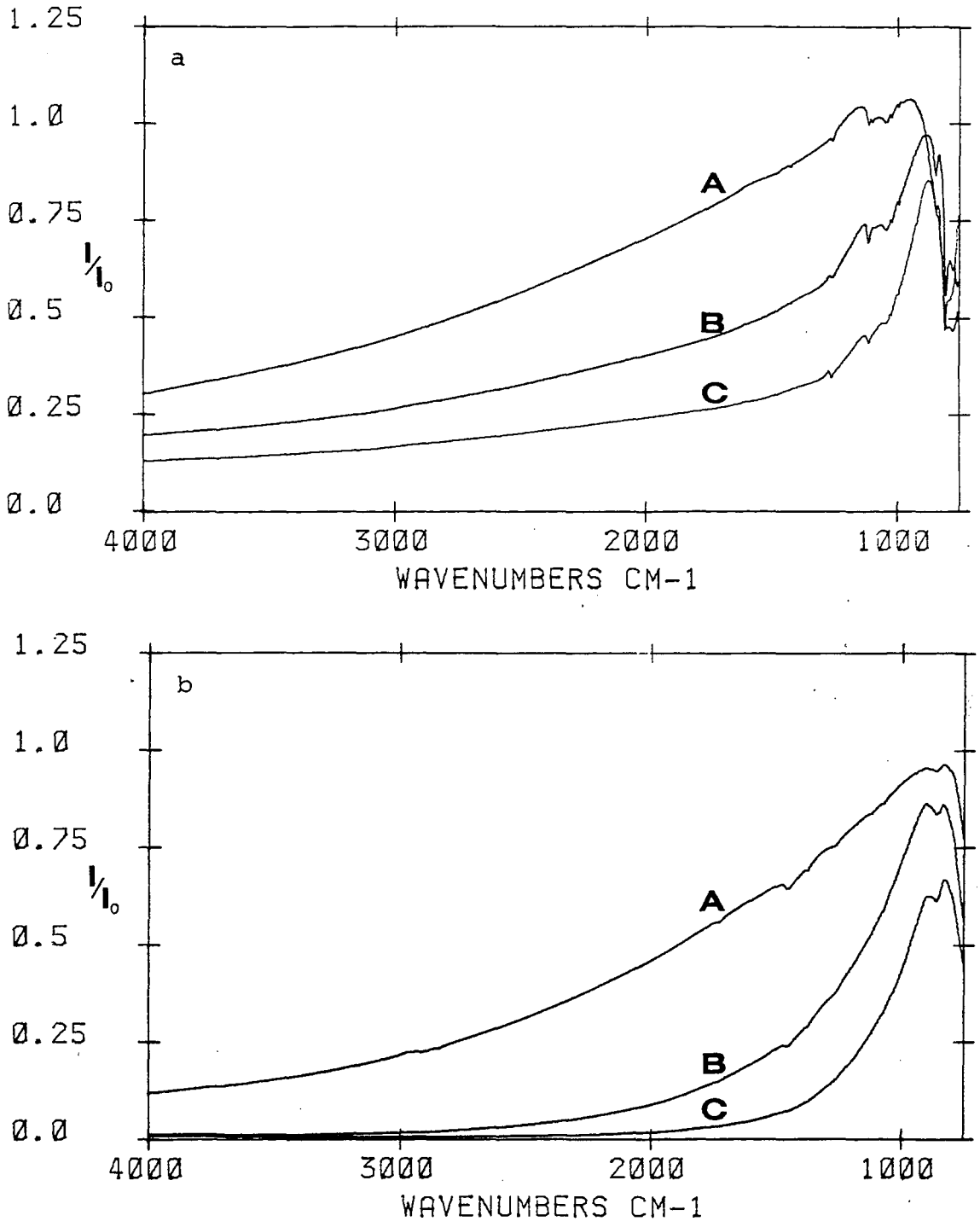


FIG. 19. (a) Spectra of (A) 0.25, (B) 0.5, and (C) 1 microns of Puratonic MgO in a copper light pipe and (b) of (A) 0.2, (B) 0.6, and (C) 1 microns of MgO smoke in a copper light pipe.

anomalous dispersion before the material reaches an adsorption band, which has been reported in the literature.[15] This assumption is also strengthened by the data of Fig. 18. Both sets of spectra are taken with $Al_2O_3$ of corresponding coverages. The 0.05 micron powder shows a much better throughput for the same thickness than the 0.3 micron powder. This can only be explained by less scattering, since all the other parameters, stayed the same. The spectra in Fig. 18 and 19 scale within 23% for an exponential dependence of the absorbance versus the thickness of the substrate in the light pipe.

Reiterating, one can say that the metal light pipe technique works only with low absorbing (non-conducting) and low scattering (small-sized) particles. Careful preparation of the sample is essential so that one achieves a pure and uniform powder. In fact, each sample should be tested before it is actually used in the cryostat.

## C. Spectra of CO Adsorbed on MgO

For the actual measurements of CO physisorbed on MgO, we used a 0.5 micron thick coating of the Puratonic MgO that had a surface area of about 25 $m^2/g$. This should lead to a ratio of 3.5 between CO molecules adsorbed on the surface and CO in the gas phase while there was still a 50% throughput (ratioed to the throughput of the clean light

pipe) of the ir beam in the region between 2250 and 1750 $cm^{-1}$. Appendix C has a complete listing of the instrumental parameters of the Bruker spectrometer. The most important were the following settings. A common mid ir source was used with a KBr beamsplitter and a liquid nitrogen detector. The aperture was 10 mm for the source and the mirror velocity was 13. The measurements were done with a resolution of 0.5 $cm^{-1}$ and 500 scans.

The measurements of CO on MgO were done on 0.5 g of Puratonic MgO that was baked at 1000° C for 48 hours at a pressure of $< 10^{-4}$ Torr. Measurements on the same MgO show that the surface area is around $25 m^2/g$ and has a coherence length of 350 A. Diffraction measurements of the MgO also show small amounts of impurities that are probably metal substitutions for Mg ions. Five mg of MgO were placed in the light pipe for the ir measurements. The same MgO was used in the light pipe and in the ballast pipe. However, the MgO was mixed with methanol for the deposition in the light pipe to determine how much was put in the light pipe and to get the substrate to stick uniformly on the walls of the light pipe. Dash *et al.* report that methanol can be completely driven off the MgO if it is baked at 500° C in a vacuum, and they report isotherm measurements on such MgO.[5]

The light and ballast pipe are then placed in the Al block and sealed off. The complete system is pumped for

another 24 hours at a pressure of less than $10^{-3}$ Torr at 75° C before any ir measurements were started.

The spectra were recorded in the following way: At first a background spectrum at room and sample temperature was stored. Any contaminations in the system should show up if those two backgrounds are ratioed, because most noninert gases would adsorb on the surface at lower temperature. Another background at sample temperature was then recorded to determine the time drift of the whole instrument. Finally, CO was put in the gas handling system to record the pressure for the VPI and then released into the light and ballast pipe. After approximately 2 hours for equilibration, the ir spectrum was taken and the equilibrium pressure recorded to determine the coverage of CO on the MgO. The last two steps were repeated until the VPI was completed. Fig. 2(b) shows the measured VPI.

Until now, we have not been able to see a spectrum of adsorbed CO on MgO or even a spectrum of any adsorbed gas on any substrate. Fig. 20 shows a typical ir spectrum of CO in the light pipe which contained MgO. The absorbance versus the pressure deviates only at higher pressures from the expected linear behavior, which is consistent with the physics. The data show that there has been adsorption in the MLP and that there was CO gas present in the light pipe. The features that show up at higher pressures as a bending of the baseline are not adsorbed features, but

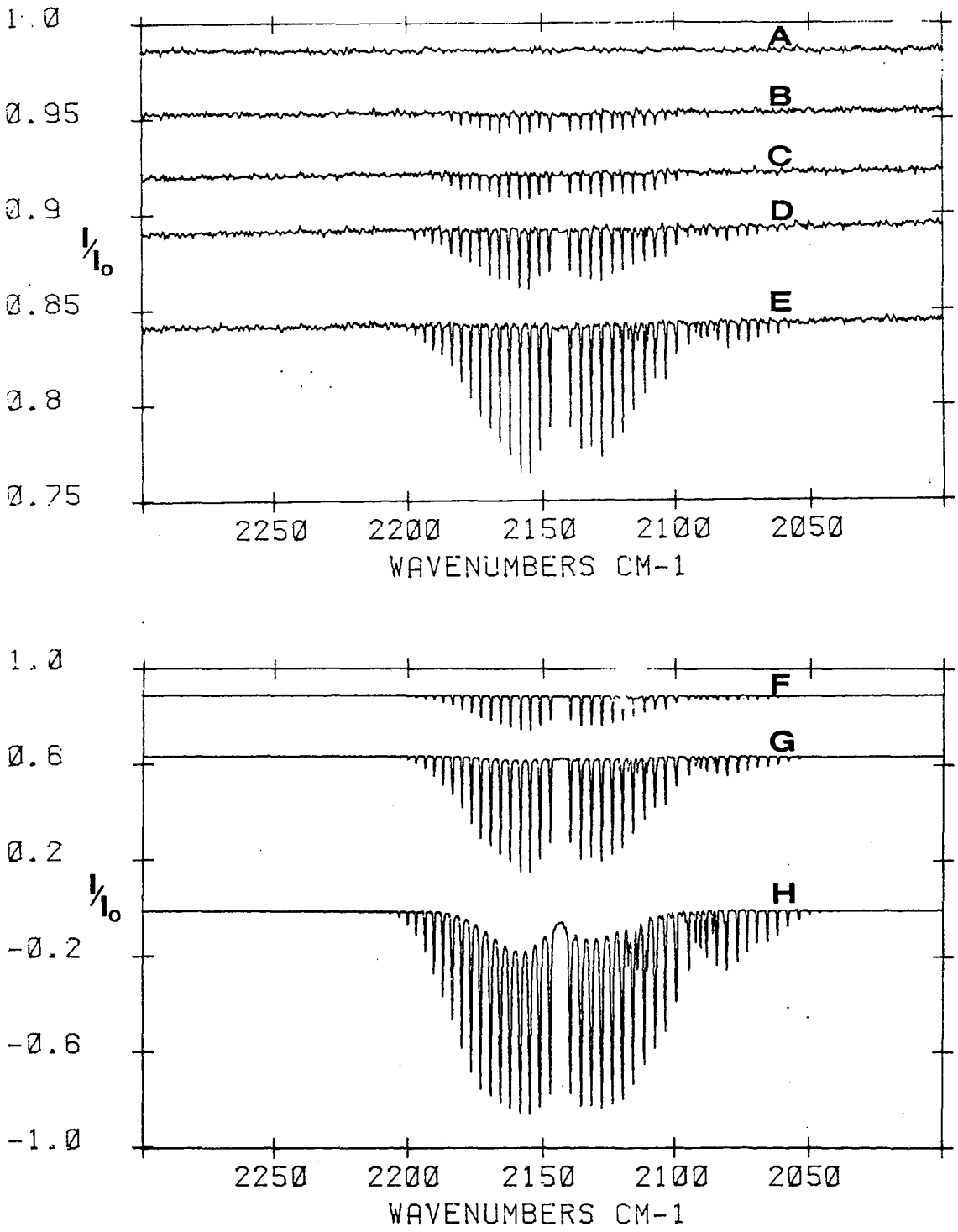


FIG. 20. Spectra of CO in a copper light pipe at T = 89 K. (A) 0.01, (B) 0.06, (C) 0.15, (D) 0.55, (E) 1.42, (F) 2.68, (G) 11.78 and (H) 40 Torr.

rather due to a broadening of the rotational absorption peak at higher pressures, since there is an interaction between the gas molecules. This feature is also reported in the literature using standard gas cells.[17] The following paragraphs will explain in words what is shown in the flowchart of Fig. 21 and try to determine why we observed no ir spectrum of adsorbed CO.

The VPI that was recorded simultaneously with the ir spectra demonstrates clearly that there has been adsorption of CO. The amount of CO can account either for the formation of bulk, if CO is not adsorbed on MgO, or for a monolayer coverage on MgO. The VPI, however, indicates again that CO adsorbed on MgO because of bulk CO would not show a step in the VPI and would not form at temperature that high. It is, therefore, very likely that the CO that was released into the system did adsorb on MgO. At present we have no other experimental way, other than the ir measurement, to determine if CO gas adsorbed just in the ballast pipe or in the light pipe also. If it would have been adsorbed in the light pipe, the spectrum of CO must have been hidden or not ir active at all. Both reasons seem very unlikely because Zecchina[24] reported spectra of CO physisorbed on MgO with sapphire windows, while our measurements showed the spectrum of MgO itself. This demonstrates that rays that could excite the CO do reach the detector and that adsorbed CO can be excited by the ir

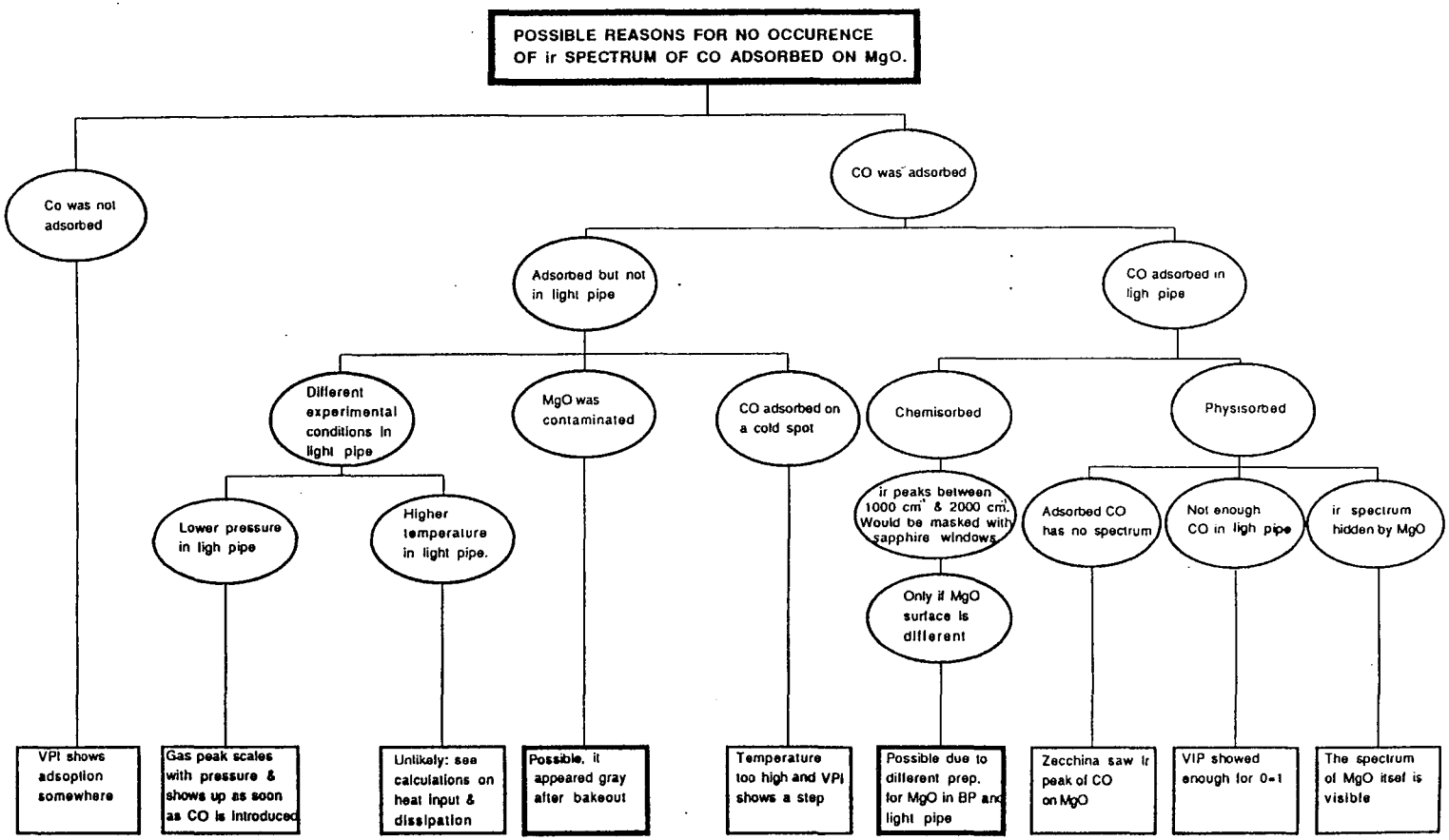


FIG. 21. Flowchart for the CO on MgO measurements.

beam.

If, however, the experimental conditions in the light and ballast pipe are different, it could be possible to record a monolayer of CO on MgO in the ballast pipe, while there is no physisorbed CO on the MgO in the light pipe. This would be virtually undetectable with a VPI because the amount of MgO in the light pipe is just 1% of the amount in the ballast pipe, while the error in the mass of the substrate in the ballast pipe is at least 2% and the precision of the VPI is at around 3%. Due to different sample conditions, CO could have adsorbed on MgO, but it could be a different type of adsorption with different ir modes. In our opinion there could be three reasons that the experimental (e.g., pressure or temperature) or sample conditions are different. First, the MgO could be different because it is prepared slightly differently, second, the ir beam could heat the light pipe and locally raise the temperature to desorb the CO, and, last, the CO could adsorb on a cold spot before it reaches the light pipe.

The last point is very unlikely because the absorbance of the gas peak correlates linearly with the pressure in the cell (Fig. 20) and shows up right after the gas is released into the system. For 11.78 Torr, for example, the ratio is (ln (100-48))/11.78 and for 40 Torr (ln (100-84))/40. This fit very well an expected exponential relation.

Local heating, however, can be a problem but should not desorb CO under our experimental conditions. Appendix D shows the calculations for the power input due to the ir beam and the dissipation for the heat due to gas conduction. The calculations indicate that an incoming ir beam of 0.2 Watts [calculated from a black body assumption with a 10 mm aperture (apt=3) and the correct geometrical corrections] should not raise the temperature of the MgO by more than 1 K at an equilibrium pressure of 2.5 Torr. The use of the smallest aperture (1.2 mm) in the spectrometer should decrease the power input by a factor of 60, and would surely not raise the temperature of the MgO significantly. It is, therefore, most likely that the MgO in the light pipe is different than the MgO in the ballast pipe. Two things could have happened to the MgO. On the one hand, the solvent could destroy the uniformity of the surface of MgO and CO would chemisorb on the surface.[3,11] The bakeout at 500° C would not correct this problem because MgO anneals at temperatures above 800° C. On the other hand, it is possible that methanol occupies the adsorption site and CO, therefore, cannot adsorb. The bakeout should eliminate this possibility.[5,21] The second possibility is that there is a metal ion exchange between Mg, Cu, and stainless steel when the Cu, light pipe is baked at 500° C with the MgO in it. This would also lead to chemisorption of CO on MgO[3]. In both cases, the spectrum of chemisorbed

CO would not be accessible with sapphire windows and would appear to us as if nothing at all is adsorbed on the MgO in the light pipe because the spectra would appear between 2000 $cm^{-1}$ and 1000 $cm^{-1}$. It is worth mentioning that we strongly believe that one of these reasons kept us from succeeding because the MgO in the light pipe looked gray after the bakeout at 500° C.

D. High $T_c$ Superconductor

The high $T_c$ superconductor material was purchased from SSC (Seattle Specialty Ceramics) and has an average size of 2 microns < $d_{50}$ < 5 microns, which means that 50% of the particles are between those limits. The material is a standard $YBa_2Cu_3O_7$ material and has a critical temperature of $T_c$ = 93 K. Diffraction measurements showed an 85% orthorombic crystal structure. $YBa_2Cu_3O_7$ was mixed with methanol so that it would stick uniformly on the inside walls of the light pipe. This technique allowed us also to determine the amount of $YBa_2Cu_3O_7$ that was put in the pipe on a volumetric basis. Following preliminary measurements, a 7.5 micron layer of $YBa_2Cu_3O_7$ was put in the light pipe so that there was still a reasonable throughput. After that, the mixture was dried in air and placed in the cryostat without further precautions. The cryostat was then--as with any other measurements--pumped out for two days at 75° C to reach a pressure of less than $10^{-3}$ Torr at room

temperature. Several thermocouples were placed on the cold surface, the light pipe, and the radiation shield to record the temperature for the first use of the dewar with liquid helium. All wires were connected to the radiation shield to reduce heat losses through the wires (see Appendix B).

Appendix C has a complete listing of the instrumental parameters of the Bruker spectrometer for the $HT_cS$ measurements. The most important were the following settings: A mercury far ir source was used with either a 23 micron or a 3.5 micron Mylar beamsplitter and a room-temperature DTGS detector. The aperture was 10 mm for the source and the mirror velocity was 2. The measurements were done with a resolution of 16 $cm^{-1}$ and either 1000 or 2000 scans.

The preferred procedure to record the spectra was the following: The dewar and the light pipe were carefully aligned to optimize the throughput. A spectrum at room temperature was recorded as a background. After that, the sample was cooled to about 110 K, to record a background above the critical temperature, and than cooled to 83 K. The spectrum at 83 K was recorded and ratioed to the one at 110 K. After that, the light pipe was heated again to 110 K to take another background and then cooled to take another sample spectrum. Fig. 22(a) shows three spectra recorded in this manner. Fig. 22(b) shows the ratio of two single beams of a superconducting state at the same

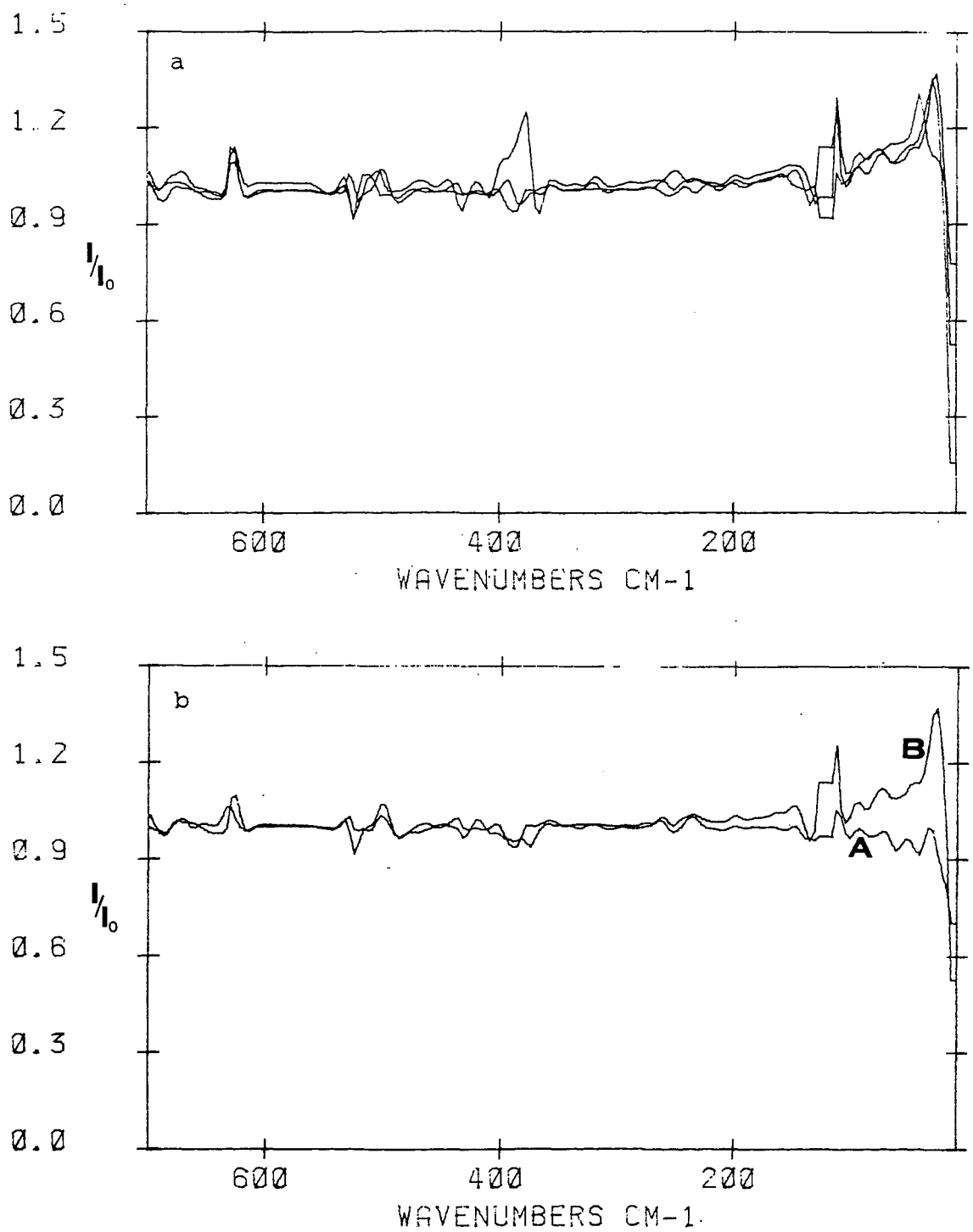


FIG. 22. Spectra of $HT_cS$: (a) three measurements with the reference beam at 110 K and sample beam at 83 K, and (b) reference beam at 110 K and (A) sample beam at 110 K and (B) sample beam at 83 K.

temperature and the ratio of two single beams from two different states. The result is that there is definitely an increase in reflectivity when $YBa_2Cu_3O_7$ turns superconducting and that the result is reproducible. The dewar was then taken out of the spectrometer, filled up with liquid helium, and realigned. Several spectra are recorded at temperatures between 30 and 110 K while the dewar was slowly warmed up. It is important that the background for all spectra was taken without moving and realigning the spectrometer to avoid errors.

The data (Fig. 23) shows the expected behavior but does not allow a precise statement about the wavelength of the energy gap. Our cutoff wavenumber is between 650 $cm^{-1}$ and 350 $cm^{-1}$, which corresponds for the ratio of the $2\ E_g/k_BT_c$ to a value between 4 and 9. This is in reasonable agreement with the literature, which records values between 8.5 and 1.2. The spectra also show an increase in reflectivity that increases when the temperature is decreased, which is consistent with the literature.

There are several problems concerning our measurements. First, the spectra are very noisy due to low intensity at certain wavenumbers. Fig. 24 shows a single beam spectrum. The intensity that reaches the detector is very low, around 130, 250, 380, 530, and above 650 $cm^{-1}$. The ratio might, therefore, vary appreciably because the sample intensity is divided by a reference intensity close

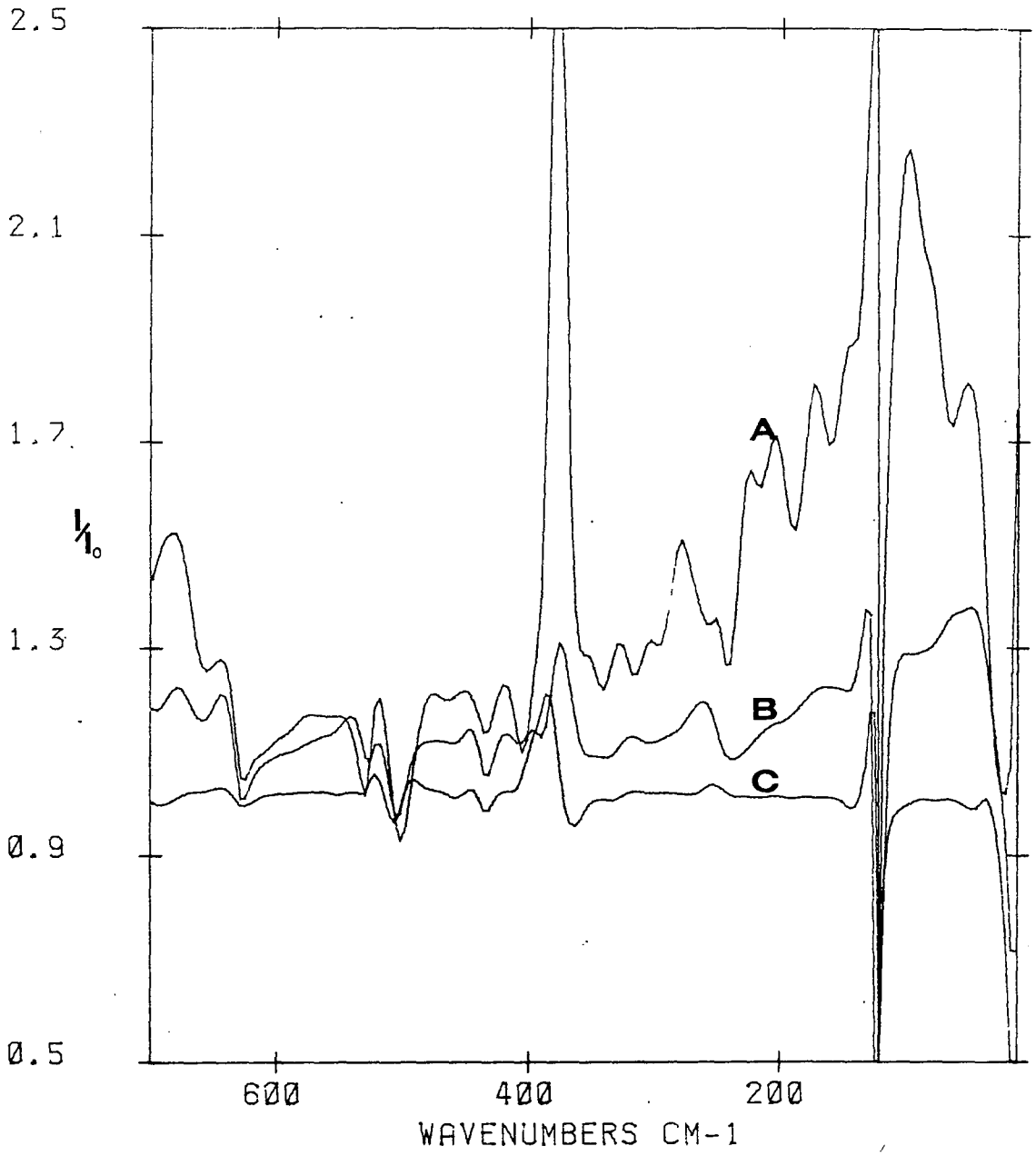


FIG. 23. Spectra of $HT_cS$ at different temperatures with the reference beam at 110 K and the sample beam at (A) 38 K, (B) 58 K, and (C) 110 K.

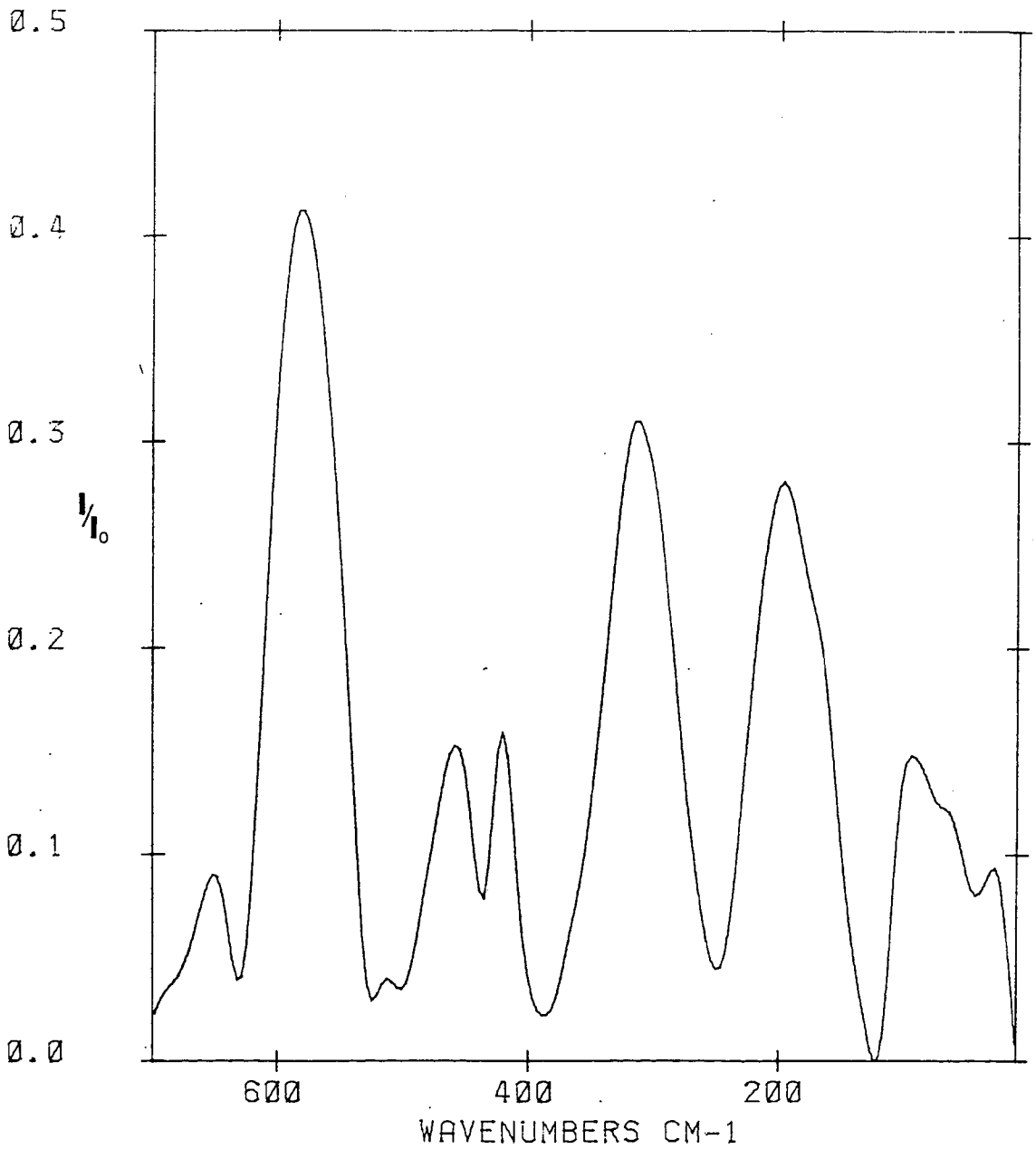


FIG. 24. Single beam spectrum for the far-ir measurements.

to zero. It is possible to improve this and also gain intensity by using a different beamsplitter (3.5 micron Mylar), but this beamsplitter masks the interesting region below 100 $cm^{-1}$. The second problem is that the background for the spectra at the coldest temperature is taken several hours after the sample spectrum. These spectra show, therefore, more noise due to drift in the source and detector. The use of a closed-cycle liquid helium refrigerator would solve the problem, because it can cycle its temperature more quickly and reproducibly. The time delay could, therefore, be reduced from more than ten hours to approximately an hour.

The last problem is the very low overall throughput. At the present, the throughput is much below our expectations even for a clean light pipe. The light pipe should transmit the ir beam better in the far-infrared than in the mid-infrared region because the wavelength is much longer. Our measurements, however, show just 10% throughput in the far-ir compared to 75% in the mid-ir. The additional layer of 7.5 micron of $YBa_2Cu_3O_7$ reduces the throughput compared to a clean light pipe by only 25%, which is consistent with the theory Fig. 25.

Summarizing, we can say that our technique works, but needs a lot improvement to make justifiable statements about the size of the energy gap.

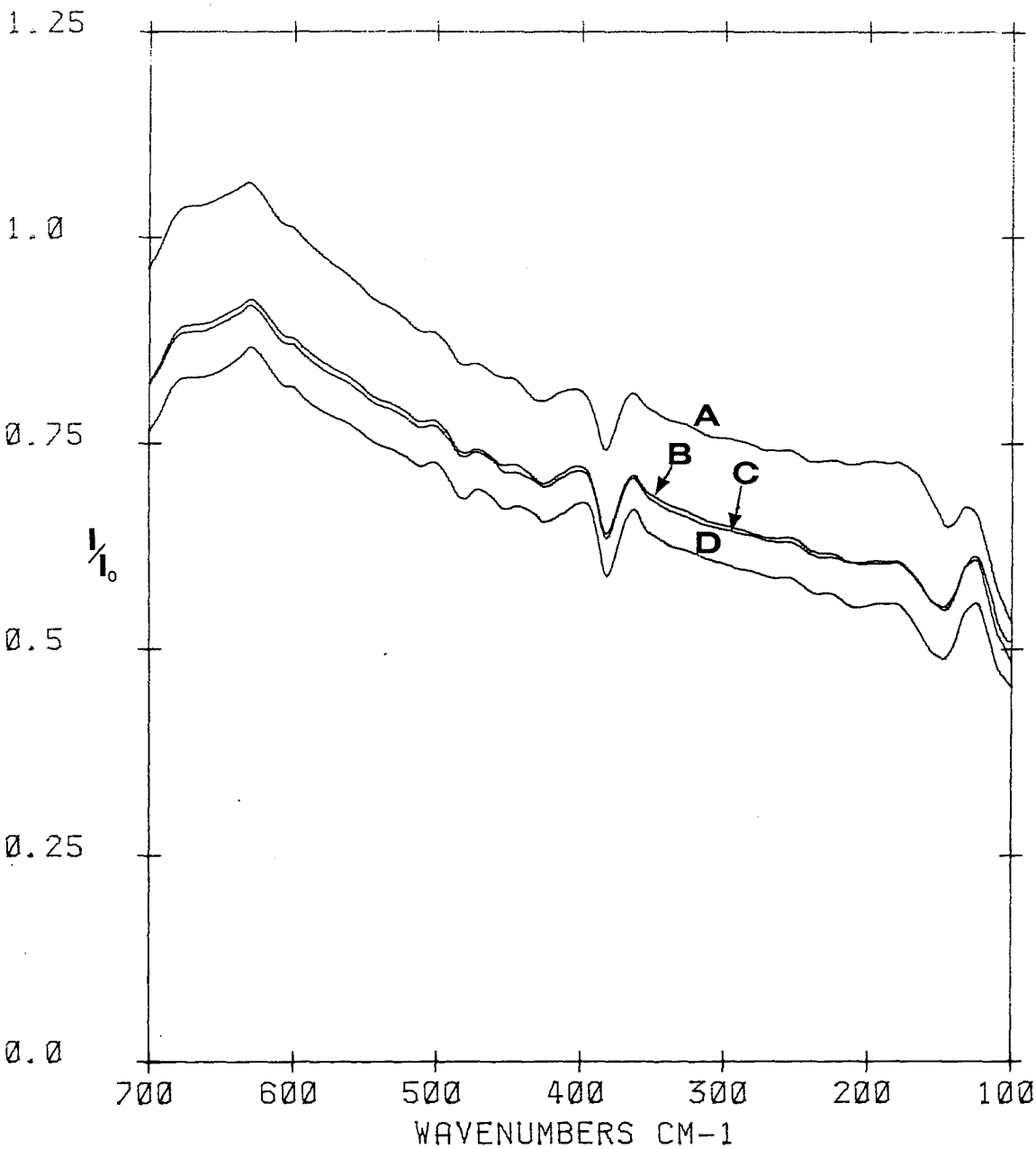


FIG. 25. Spectra of different thicknesses of $YBa_2Cu_3O_7$: (A) 1, (B) 2, (C) 5, and (D) 10 microns of $YBa_2Cu_3O_7$.

# CHAPTER V

# CONCLUSION

This chapter summarizes the major results and accomplishments presented in this thesis. It also provides suggestions for short-term and long-term improvements of the instrumentation and for experiments in the future.

The main accomplishment of the research is that the design and the construction of the extended MLP instrument has been completed and the instrument is functional. The method of the metal light pipe is definitely applicable for energy gap measurements of high $T_c$ superconductors and seems to be applicable for measurements of adsorbed gases on high-surface-area materials. Even while the latter has not been seen yet with the instrument, it seems more likely to be more of a problem with the sample preparation than with the technique or the instrumentation.

The gas handling system has proven its capability in several experiments and only needs improvement of its accuracy and precision. There are four points of improvement: The recallibration of the standard volumes; enclosure of the whole system in thermal insulation; a higher accuracy differential pressure manometer; and automation of the whole system. The first improvement would just improve the accuracy in the instrument, which

to improve the absorption measurements by optimizing all the experimental parameters, such as sample preparation, the liquid helium environment, and the spectrometer itself. These adjustments can be made while one investigates CO-CO interaction, phase transitions, and the adsorption of CO on defects of MgO substrate. After this, one should be in good position to try the investigation of low-energy collective phonon excitation of CO on MgO. When a thorough study of the CO/MgO system has been completed, one could try to adsorb different gases on MgO. Nitrogen would determine if ir measurements are possible on gases that have no permanent electric dipole[28] but only an induced dipole when adsorbed on the substrate. Methane represents an organic gas adsorbed on MgO, whose structure has already been studied considerably.[4] All these measurements would investigate the bonds between adsorbates and substrate and would lead to a better understanding of bonding between surfaces. The technique would greatly enhance the availability of different tools to measure those bonds and, therefore, add to surface science as a whole.

# REFERENCES

1. D. A. Bonn, J. E. Greedan, C. V. Stager, M. G. Doss, S. L. Herr, K. Kamarás, and D. B. Tanner, Phys. Rev. Lett., 2249 (1987).

2. J. C. Clark, P. B. Chilson, and G. G. Ihas, Rev. Sci. Instrum., **61**, 3621 (1990).

3. E. A. Colbourn and W. C. Mackrodt, Surf. Sci., **143**, 391 (1984).

4. J. P. Coulomb, K. Madih, B. Croset, and H. J. Lauter, Phys. Rev. Lett., **54**, 1536 (1985); J. M. Gay, A. Bienfait, J. P. Coulomb, J. Suzanne, H. Blank, and P. Convert, Physica B, **156 & 157**, 273 (1989); K. Mardih, B. Croset, and H. J. Lauter, Europhys. Lett., **8**, 459 (1989).

5. J. G. Dash, R. Ecke, J. Stoltenberg, O. E. Vilches, and J. Whittemore, Jr., J. Phys. Chem., **82**, 1450 (1978).

6. R. Dovesi, R. Orlando, F. Ricca, and C. Ricca, Surf. Sci., **186**, 267 (1987).

7. L. Forro, G. L. Carr, G. P. Williams, D. Mandrus, and L. Mihaly, Phys. Rev. Lett., **65**, 1941 (1990).

8. S. Furuyama, H. Fujii, M. Kawamura, and T. Morimoto, J. Phys. Chem., **82**, 1028 (1978).

9. E. Garonne, A. Zecchina, and F. S. Stone, J. Chem. Soc. Faraday Trans. 1, **84**, 2843 (1988).

10. R. Gevirzman, Y. Kozirovski, and M. Folman, Trans. Faraday Soc., **65**, 2206 (1969).

11. E. Guglieminotti, S. Coluccia, E. Garrone, L. Cerruti, and A. Zecchina, Surf. Sci., **158**, 378 (1984).

12. Halliday Resnik, *Fundamentals of Physics*, 3rd ed. (Wiley, New York, 1988).

13. W. N. Hansen, J. Opt. Soc. of America, **58**, 380 (1968).

14. W. N. Hansen and G. J. Hansen, Appl. Spectrosc. **41**, 553 (1987).

15. W. N. Hansen, J. F. Andrew and G. J. Hansen, Appl. Spectrosc. **41**, 562 (1987).

16. W. Herres and J. Gronholz, "Understanding FT-IR Data Processing," Bruker Analytische Messtechnik GmbH, West Germany (1987).

17. G. Herzberger, *Molecular Spectra and Molecular Structure*, (van Nostrand, Princeton, New Jersey, New York, 1945).

18. K. Kamarás, S. L. Herr, C. D. Porter, N. Tache, and D. B. Tanner, Phys. Rev. Lett. **64**, 84 (1990).

19. J. R. Kirtley, R. T. Collins, Z. Schlesinger, W. J. Gallagher, R. L. Sandstorm, T. R. Dinger, and D. A. Chance, Phys. Rev. B, **35**, 8846 (1987).

20. C. C. Lim, Rev. Sci. Instrum., **57**, 108 (1986).

21. K. Morishige, S. Kittaka, and T. Morimoto, J. Coll. Interface Sci. **89**, 86 (1982).

22. Omega Engineering, *OMEGA Complete Temperature Measurement Handbook and Encyclopedia*, (Omega Engineering, Stamford, CT, 1988).

23. Mario Pineda, unpublished research paper.

24. E. E. Platero, D. Scarano, G. Spoto, and A. Zecchina, Faraday Discuss. Chem. Soc., **80**, 183 (1985).

25. H. H. Richardson, G. E. Ewing, J. Phys. Chem., **90**, 5834 (1987).

26. A. G. Shastri, H. B. Chae, M. Bertz, J. Schwank, J. Phys. Chem., **89**, 3761 (1985).

27. Z. Schlesinger, R. L. Green, J. G. Bednorz, and K. A. Müller, Phys. Rev. B, **35**, 5334 (1987).

28. Z. Schlesinger, R. T. Colins, F. Holtzberg, C. Feild, H. Blanton, U. Welp, G. W. Crabtree, Y. Fang, and J. Z. Liu, Phys. Rev. Lett., **65**, 801 (1990).

29. R. M. Suter, N. J. Colella, R. Gangwar, and W. Wang, Rev. Sci. Instrum., **58**, 462 (1987).

30. M. Trenary and M. E. Brubaker, J. Chem. Phys., **85**, 6100 (1986).

31. G. K. White, *Experimental Techniques in Low-Temperature Physics*, 3rd ed. (Oxford Science, Oxford, 1979).

32. H. Ye, W. Lu, Z. Yu, X. Shen, B. Miao, Y. Cai, and Y. Qian, Intern. J. Mod. Phys. B., **1**, 503 (1987).

33. D. M. Young and A. D. Crowell, *Physical Adsorption of Gases*, (Butterworths, Washington, 1962).

34. A. Zecchina, D. Scarano, and E. Garrone, Surf. Sci. **160**, 492 (1985).

# APPENDICES

# Appendix A: Gas Handling System

## A.1 System Hardware

The gas handling manifold was built from four 1/8" NPT Stainless Steal crosses that are connected with 1/8" NPT couplers (Fig. 26). Stainless steel is used because it is a strong material and does not outgas or corrode. Teflon is used as a sealing material between any threaded parts. Eight of the ten openings are connected to Whitney Teflon sealed stainless steal valves to protect pressure sensors or seal off certain ports. Whitney specifies their vacuum capabilities to less than $10^{-5}$ Torr. The other two ports (E, J in Fig. 26) are connected to a thermocouple gauge and to a pressure relief valve that opens at an overpressure of approximately 3 atmospheres. Both devices need not be valved off from the system. At the present, the thermocouple is used to determine when the system is completely pumped out because it can measure the best vacuum in the system. The relief valve serves two functions. It should release the pressure if a sample cell warms up, releasing a lot of gas adsorbed on its substrate. It also protects the capacitance manometer if the gas handling system is overpressured during the filling procedure.

The main pressure gauge (I) is an absolute capacitance manometer (MKS model A122). The digital readout (MKS model

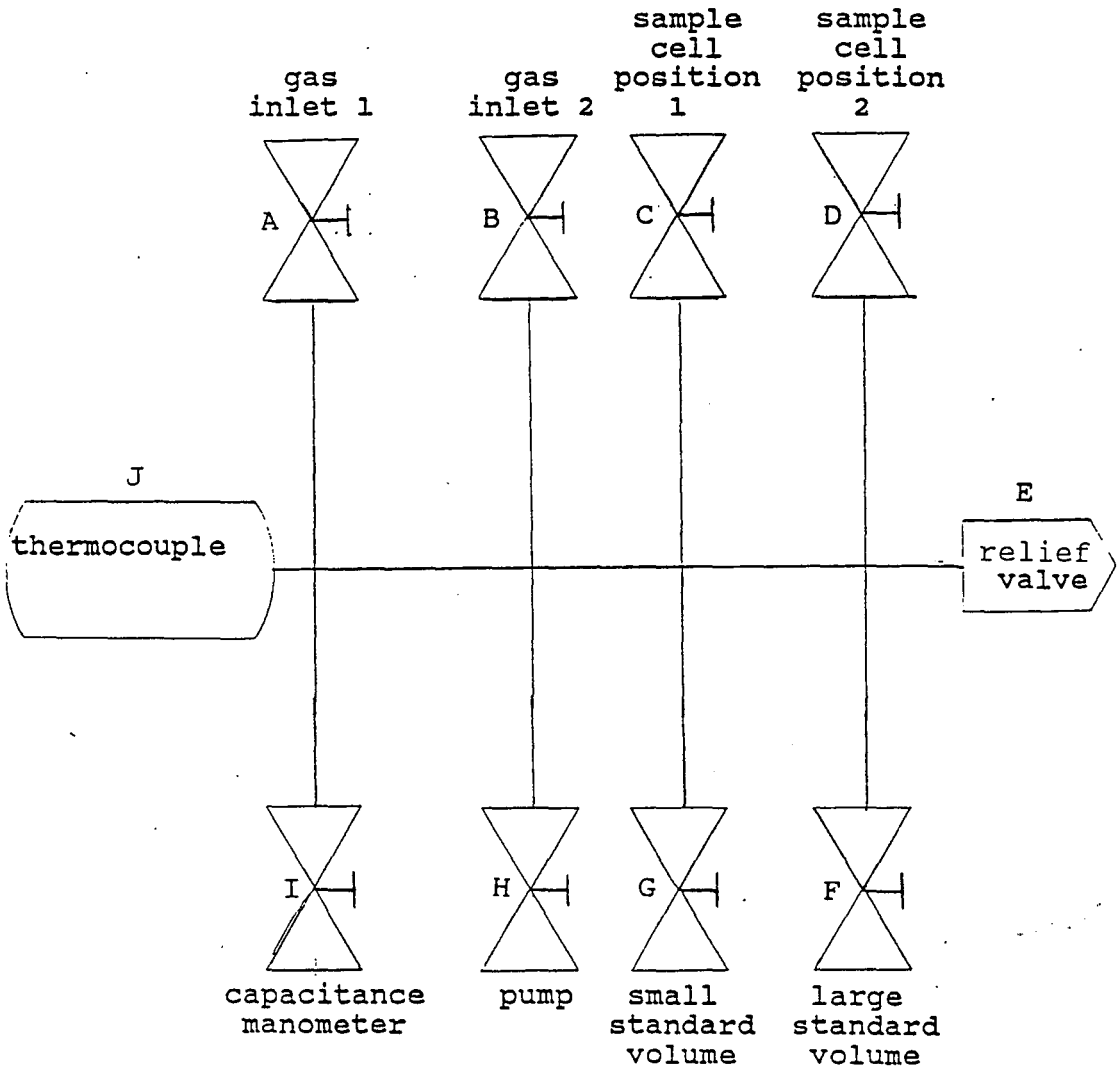


FIG. 26. Schematic of the gas handling system.

PDR 1) provides power to the gauge and reads the pressure. The reference side of the pressure gauge is sealed off, and the whole system is calibrated by MKS to +/- 0.01 Torr. The maximum measurable pressure is 100 Torr, while the lowest is 0.01 Torr. Capacitance manometers operate on the principle that the capacitance of two surfaces depends on their separation. A diaphragm separates the evacuated reference side from the side that is connected to the gas handling system. The diaphragm deflects, depending on the pressure in the gas handling system, and relates the deflection to a capacitance. The gas handling system is designed to allow an upgrade with a higher accuracy differential pressure gauge, which should improve its performance significantly.

The two standard volumes (G, F) usually contain reserves of the adsorbate gas, but were also used to calibrate the system. If the volume of the manifold is too small, because one uses a large amount of a high-surface adsorbent, one of the standard volumes can be added to the manifold. The stainless steel standard volumes have, therefore, different volumes to allow different manifold volumes.

Two (C, D) of the other five ports are used as connections to sample cells, while the remaining three are used as gas inlets (A, B) and to connect to a vacuum pump (H).

The temperature of the gas handling system is measured by a type K thermocouple within an accuracy of +/- 0.1 K to compensate for changes in the room temperature.

## A.2 System Calibration

The gas handling system was calibrated by expanding a known volume of gas into the volume to be calibrated. The ideal gas equation relates, then, the initial and final pressures to the initial and final volumes.

To start, it is therefore important to precisely calibrate one or two standard volumes. Our calibration was done gravimetrically by weighing the standard volumes empty and weighing them again after they were filled with methanol. 233.5 g +/- 0.2 g of methanol filled the large cell while only 31.56 g +/- 0.02 g fit in the small cell.

The density of the solvent was calculated to 0.789 $g/cm^3$ +/- 0.001 $g/cm^3$, which lead to the following volumes for the standard cells. The errors for the volumes include accuracy and precision, where the accuracy accounts always for 0.2% of the error.

$V_{lg}$ = 295.8 $cm^3$ +/- 0.7 $cm^3$ rel. uncertainty = 0.2%

Vsm = 39.98 $cm^3$ +/- 0.08 $cm^3$ rel. uncertainty = 0.2%

Those calibrated standard volumes lead in turn to the following volumes of the gas manifold. Each volume

calibration was done with six measurements with both standard volumes.

$V_{gas\ handling}$ = 47.17 $cm^3$ +/-0.1 $cm^3$ rel. uncertainty = 0.24%

The volume of the capacitance manometer and the valve was than calibrated with the gas handling volume.

$V_{manometer}$ = 9.42 $cm^3$ +/-0.02 $cm^3$ rel. uncertainty = 0.27%

$V_{valve}$ = 0.047 $cm^3$ +/- 0.001 $cm^3$ rel. uncertainty = 2%

## A.3 System Problems and Improvements

The system could be improved in certain aspects. The error in the adsorbed volume is at the moment at approximately 3%. The temperature drift, accounting for 0.7% of the error, could be reduced to about 0.1 by enclosing the whole system in an insulating material, such as styrofoam. The uncertainty in the standard volumes and, therefore, the resulting uncertainties in all the other volumes, could be reduced substantially from 0.2% to 0.05% by recalibrating the standard volumes. The recalibration should then be done with a fluid of exactly known density and with a better temperature stability. Last, the use of a high-accuracy differential gauge would improve the system performance. Since the uncertainty of the pressure accounts for more than half of the total error (1.7%) it should be improved with a high-accuracy pressure gauge. The other errors, such as the temperature correction of the

pressure gauge itself, are small compared to the mentioned ones. The uncertainty in the standard volumes is at the moment the biggest uncertainty in absolute measurements, with an error of 0.2% per data point, but far below the precision of the instrument with 3%. It is, however, evident that an upgrade of the system with a better pressure gauge should be accompanied by insulating it against drift in the room temperature. Automation of the whole system would also mitigate human impatience, which sometimes records a data point before it is equilibrated.[29]

## Appendix B: Calculation of the Cryostat Heat Losses

The holding time for a cryostat depends on the heat losses that the cryostat experiences. Following the treatment in White's book,[31] there are three sources for heat losses. The first one is due to conduction of residual gas or feedthroughs, the second is due to radiation, and the last is due to convection. In our system there will be an additional heat loss due to the power of the incoming ir beam, which gets partially adsorbed in the cryostat. I will give the results for the first two because convection cannot take place at the pressure that we are dealing with. The mean free path is around 10 cm at $10^{-1}$ Pascal so that there will be almost no convection in the cryostat.

The calculations for the heat losses are done in three parts; first for the liquid nitrogen shield (T=100 K), second for the cold surface at liquid nitrogen temperature (T=78 K) while the shield is at 100 K, and third for the cold surface at liquid helium temperature (T=20 K) while the shield is at 100 K.

The following calculations show that for the liquid nitrogen shield the biggest leak is due to the residual gas pressure of $10^{-1}$ Pascal. Radiation losses and conduction through the wires of the heaters and the temperature sensor have almost no effect. The theoretical holding time of

liquid nitrogen in the shield reservoir agrees with the experimental holding time very well.

The calculations of the holding time for the shielded cold surface at 78 K does also agree with the experimental data in the limits of our measurements. The calculations show a holding time of 6 days, but we never ran experiments for more than 2 days. The biggest factors are due to the gas conduction and the ir beam.

The comparison between the calculations and the experiments of the holding time for liquid helium are very vague because there is only one experimental data point. A holding time of 3 hours was calculated, while we reached 3.5 hours in the experiment. It is questionable if we reached the limit of the holding time because it was our first try and the set-up was not optimized.

Table 2 summarizes the results of the calculations, while the calculation for the power of the ir beam can be found in Appendix D. Appendix D shows that the power input from the ir source can be easily reduced if one uses asmaller aperture. The maximum reduction is about a factor of 60 in the ir beam. The calculations follow the teatment in White's book, "Experimental Techniques in Low-Temperature Physics," Chap. 5. All the necessary constants and assumptions can also be found in this book.

TABLE 2: Power input and holding time for the cryostat.

| | Shield at 100 K | Cold surface at 78 K with shield at 100 K | Cold surface at 20 K with shield at 100 K |
|---|---|---|---|
| Power due to residual gas conduction | ($P=10^{-1}$Pa) 4.2 W | ($P=10^{-1}$Pa) 0.4 W | ($P=10^{-2}$Pa) 0.1 W |
| Power due to conduction of the feed-throughs | 0.1 W | 0.04 W | 0.1 W |
| Power due to radiation | $10^{3}$ W | $10^{-5}$ W | $10^{-3}$ W |
| Power of the absorbed ir Beam (See Appendix C) | 0 W | 0.2 W | 0.2 W |
| Total power input | 4.3 W | 0.6 W | 0.5 W |
| Theoretical holding time for cryogen | (1.5 lit l-$N_2$) 15 hours | (2 lit l-$N_2$) 6 days | (2 lit l-He) 3 hours |
| Experimentally measured holding time | 16 hours | > 2 days | 3.5 hours |

Appendix C: Parameter Listing for the 113V Bruker Spectrometer

Parameter listing for the far-ir measurements of high $T_c$ superconductors:

```
INFO FOR FILE  T1113S05.DATA
SPECTRUM FILE
MEASURED ON IFS 113
DATE 13/11/90   TIME 13:17:30   RSN=8415        ZFF=2   NPT=180
SCN=500 PKL=177 SCL=1   FFP=702.050781  FLP=7.714844
GAIN=5  SSP=1   PKA=683
CNM=UTAH STATE  SNM=MCT SFM=KBR PELLET 00       RES=16.0
APT=3   BMS=4   DTC=FI  GSG=1   GSD=0   AQM=SN  COR=NO  HPF=7   LPF=5
OPF=1   RCH=BK  RNR=0   SCH=BK  SNR=0   SRC=FI  VEL=2   APF=HG  WDS=0.0
WDE=0.0
```

Parameter listing for the mid-ir measurements of CO adsorbed on MgO:

```
INFO FOR FILE  T1025S06.DATA
SPECTRUM FILE
MEASURED ON IFS 113
DATE 25/10/90   TIME 13:32:42   RSN=8275        ZFF=2   NPT=9334
SCN=250 PKL=169 SCL=0   FFP=4000.146484 FLP=1749.822998
GAIN=2  SSP=1   PKA=4578
CNM=UTAH STATE  SNM=MCT SFM=KBR PELLET 00       RES=0.5
APT=2   BMS=6   DTC=MI  GSG=1   GSD=0   AQM=SN  COR=NO  HPF=2   LPF=1
OPF=1   RCH=FT  RNR=0   SCH=BK  SNR=0   SRC=FI  VEL=15  APF=HG  WDS=0.0
WDE=0.0
```

Appendix D: Calculation of the Power Input
Due to the ir Source and Its Dissipation

The power input from the ir source can be calculated by using a black body assumption and the Stefan-Boltzmann law.

Symbols:

$W_{source}$ is the radiation power that is emitted from the mid-ir source in the solid space angle

$W_{MLP}$ is the power input into the light pipe

A is the area of the aperture in $m^2$

T is the temperature of the mid-ir source in Kelvin

$\sigma$ is the Stefan-Boltzmann constant

$\delta\Omega$ is the solid angle in space

Constants:

$A = 0.005 \cdot \pi \quad m^2$

$T = 1400 \quad K$

$\sigma = 5.67 \cdot 10^{-8} \quad W/m^2 K$

$\beta_{BMS} := 0.25$

$\beta_{KBr} := 0.85$

$\beta_{SAP} := 0.85$

$$\delta\Omega := \frac{\int_{-\frac{\pi}{6}}^{\frac{\pi}{6}} \cos(\alpha)\, d\alpha}{4 \cdot \pi}$$

Equations:

$$W_{source} := \sigma \cdot A \cdot T^4$$

$$W_{MLP} := W_{source} \cdot \delta\Omega \cdot \beta_{BMS} \cdot \beta_{KBr} \cdot \beta_{SAP}$$

Results:

$$W_{source} = 17. \quad W$$

$$W_{MLP} = 0.25 \quad W$$

Heat transfer between the light pipe and the MgO due to the gas in the light pipe:

$$P_{gas} = c \cdot a_0 \cdot P \cdot \delta T \cdot A$$

| | |
|---|---|
| $c = 1.2$ | numerical constant |
| $a_0 = 0.8$ | constant for air |
| $P = 300 \ Pa$ | pressure in MLP |
| $\delta T = 1 \ K$ | temperature difference |
| $A = 0.0015 \cdot 0.1 \cdot 2 \cdot \pi \ m^2$ | area of the MLP |

$$P_{gas} = 0.3$$

We can assume that the Mgo does not rise for more than 1K, because the heat conduction due to the gas is larger than the power input from the ir source, under the assumed conditions.